

Development of Novel Antibacterial Ti-Nb-Ga Alloys with Low Stiffness for Medical Implant Applications

By
Rhianna McHendrie

*Thesis
Submitted to Flinders University
for the degree of*

**Bachelor of Science (Honours) (Chemical Sciences)/
Master of Engineering (Materials)**
College of Science and Engineering
October 2023

TABLE OF CONTENTS

TABLE OF CONTENTS	I
ABSTRACT	III
DECLARATION	IV
ACKNOWLEDGEMENTS	V
LIST OF FIGURES	VI
LIST OF TABLES	VIII
LIST OF PUBLICATIONS	IX
1.0 INTRODUCTION	1
2.0 LITERATURE REVIEW	3
2.1 New generation titanium alloys with biocompatible elements.....	3
2.1.1 Influence of alloying elements on microstructure and mechanical properties	3
2.1.2 Influence of alloying elements on biocompatibility.....	4
2.2 Antibacterial Gallium-based materials.....	5
2.2.1 Gallium in bioglasses.....	5
2.2.2 Gallium in liquid metals.....	7
2.2.3 Gallium in bioceramic systems	7
2.3 Titanium-Gallium based systems.....	8
2.3.1 Titanium-Gallium coatings	8
2.3.2 Titanium-Gallium based alloys.....	10
3.0 METHODOLOGY	12
3.1 Alloy Composition Design	12
3.2 Sample Fabrication & Preparation	12
3.2.1 Alloy Casting.....	12
3.2.2 Sample Preparation.....	13
3.3 Microstructural Characterisation	14
3.3.1 Optical Microscopy	14
3.3.2 SEM and EDS	14
3.4 Mechanical Characterisation.....	14
3.4.1 Microhardness.....	14
3.4.2 Nanoindentation	14
3.5 Biological Characterisation.....	15
3.5.1 Antimicrobial Activity Assay.....	15
3.5.2 Cytotoxicity Assay	16
3.5.2.1 F-actin Staining.....	17
3.5.3 Statistical Analysis.....	17
4.0 RESULTS	18

4.1	Microstructural Characterisation	18
4.1.1	Optical Microscopy	18
4.1.2	SEM and EDS	19
4.2	Mechanical Characterisation.....	23
4.2.1	Microhardness	23
4.2.2	Nanoindentation	24
4.3	Biological Characterisation.....	26
4.3.1	Antimicrobial Activity Assay.....	26
4.3.2	Cytotoxicity Assay	28
5.0	DISCUSSION	30
5.1	Microstructural and Mechanical Evaluation	30
5.2	Biological Evaluation	33
5.3	Limitations of this Study	35
6.0	CONCLUSIONS & SUGGESTIONS FOR FUTURE WORK	36
6.1	Conclusions.....	36
6.2	Suggestions for Future Work	37
REFERENCES		38
APPENDICES		43
Appendix A.....		43
Appendix B.....		45
Appendix C.....		46
Appendix D.....		47
Appendix E.....		49

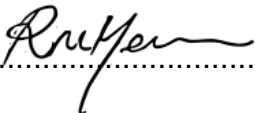
ABSTRACT

With the rising demand for implantable orthopaedic medical devices and the dominance of device-associated failures including infections, extensive research has been prompted into the development of novel biomaterials that can offer desirable characteristics. This thesis therefore aims to design and develop new titanium-based alloys containing minor gallium additions with the aim of offering beneficial antibacterial properties while having a reduced stiffness level to minimise the effect of stress shielding when in contact with bone. This study focuses on the microstructure, mechanical properties, antimicrobial activity, and cytocompatibility to inform the suitability of the designed alloys as orthopaedic biomaterials. Novel Ti-33Nb-xGa alloys ($x = 3, 5$ wt%) were produced via casting followed by homogenisation treatment, where all results were compared to the currently employed orthopaedic alloy Ti-6Al-4V. Optical microscopy, scanning electron microscopy (SEM) and energy dispersive spectroscopy (EDS) results depicted a single beta (β) phase microstructure in both alloys, where Ti-33Nb-5Ga was also dominated by dendritic alpha (α) phase grains in a β -phase matrix. EDS analysis indicated that the α -phase dendrites in Ti-33Nb-5Ga were enriched with titanium, while the β -phase was richer in niobium and gallium elements. Differences in the single β -phase grains were mapped with an inverse pole figure (IPF) and were attributed to variances in crystal structure orientations. Mechanical properties were measured using nanoindentation and microhardness methods, where the Young's modulus for Ti-33Nb-3Ga and Ti-33Nb-5Ga was found to be 75.4 ± 2.4 and 67.2 ± 1.6 GPa respectively, a significant improvement of 37.4% and 44.2% over Ti-6Al-4V. Importantly, both alloys achieved superior antimicrobial properties against Gram-negative *P. aeruginosa* and Gram-positive *S. aureus* bacteria. Antibacterial efficacy was noted at up to $90 \pm 5\%$ for the 3 wt% alloy and $95 \pm 3\%$ for the 5 wt% alloy. These findings signify an important enhancement of the antimicrobial performance by as much as 130.3% and 187.8% when compared to Ti-6Al-4V. No cytotoxicity was observed in hGF cell lines over 24 hours. Cell morphology and cytoskeleton distribution appeared to depict typical morphology with a prominent nucleus, elongated fibroblastic spindle-shaped morphology, and F-actin filamentous stress fibres in a well-defined structure of parallel bundles along the cellular axis. The developed alloys in this work have shown very promising results and are suggested to be further examined towards the use of orthopaedic implant components.

DECLARATION

I certify that this thesis:

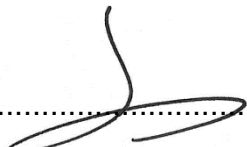
1. does not incorporate without acknowledgment any material previously submitted for a degree or diploma in any university
2. and the research within will not be submitted for any other future degree or diploma without the permission of Flinders University; and
3. to the best of my knowledge and belief, does not contain any material previously published or written by another person except where due reference is made in the text.

Signature of student.....

Print name of student.....Rhianna McHendrie.....

Date.....23 Oct 2023.....

I certify that I have read this thesis. In my opinion it is ~~is not~~ fully adequate, in scope and in quality, as a thesis for the degree of Bachelor of Science (Honours) (Chemical Sciences)/ Master of Engineering (Materials). Furthermore, I confirm that I have provided feedback on this thesis and the student has implemented it ~~minimally/partially~~ fully.

Signature of Principal Supervisor.....

Print name of Principal Supervisor.....Reza Hashemi.....

Date.....23 Oct 2023.....

ACKNOWLEDGEMENTS

I would like to express my deepest appreciation to my supervisor, Dr Reza Hashemi, for his continued support, guidance, and expertise that has made my masters project an inspiring experience that would not have been possible without him. Additionally, I could not have undertaken this endeavour without my co-supervisor Dr Vi Khanh Truong, who generously provided his knowledge and assistance throughout the duration of this project. My sincere thanks are also owed to Flinders University for their facilities and generous financing of my research.

I would also like to extend my thanks to Mr Tim Hodge and PhD students Ngoc Huu Nguyen and Manh Tuong Nguyen for their assistance and expertise. Furthermore, I am also thankful to Microscopy Australia at Flinders University Microscopy and Microanalysis, in addition to Adelaide Microscopy at Adelaide University, for their facilities and scientific and technical assistance.

Finally, I wish to acknowledge my family and friends for their ongoing support and encouragement, especially to my mother Ms Belinda Jones.

LIST OF FIGURES

Figure 1: Scanning electron microscopy (SEM) images for (a) Ti-23Nb-7Zr, (b) Ti-28Nb-7Zr, and (c) Ti-33Nb-7Zr at 15,000x magnification [28].	4
Figure 2: Comparison of elastic modulus and UTS of the Ti-35Nb-2Ta-3Zr alloy compared to other alloys developed in literature [29].	4
Figure 3: The osteoblast viability after 1, 4, 8 and 16 days on samples of Ti-6Al-4V (control) and Ti-35Nb-2Ta-3Zr. Data is expressed as mean \pm standard deviation [19].	5
Figure 4: Bacterial survival of <i>S. aureus</i> after 24 hrs of (1) seeded colony forming units (CFUs); (2) control sample; (3) bare and silica-rich; (4) SiO ₂ -CaO-P ₂ O ₅ -MgO-CaF ₂ sample; (5) Cu and Ga coated SiO ₂ -CaO-P ₂ O ₅ -MgO-CaF ₂ substrate [35].	6
Figure 5: a) Results of Ga ₂ O ₃ -doped phosphate-based glasses in 0, 1, 3 and 5 mol % using a disc diffusion assay against <i>S. aureus</i> , <i>E. coli</i> , <i>P. aeruginosa</i> , methicillin-resistant <i>S. aureus</i> , and <i>C. difficile</i> . b) The viability of <i>P. aeruginosa</i> from 0, 1, and 3 mol % Ga ₂ O ₃ -doped phosphate-based glasses after 4, 12 and 24 hrs [39].	6
Figure 6: Control and magnetically activated (treated) gallium-based LM against <i>P. aeruginosa</i> and <i>S. aureus</i> : (A) Raw colony-forming unit (CFU), and (B) logarithmic CFU depiction [48].	7
Figure 7: The live/dead biofilm biomass (%) of <i>A. baumannii</i> after 7 days from (a) control Ti, (b) Ti with Ga-containing calcium titanate, and (c) Ti with gallium titanate (GT) [56].	9
Figure 8: Release of antibacterial activity against <i>A. baumannii</i> measured over 21 days (a) Silver release from AgCis and AgNPS (b) gallium release from GaCis and GaOss [14].	10
Figure 9: Antibacterial effect of the Ti-8Al-3Si-3Zr-(1, 2, 20 wt%)-Ga alloys and control samples: (a) metabolic activity at 24, 48, 72 h of <i>S. aureus</i> , (b) metabolic activity over time of <i>S. aureus</i> , (c) <i>S. aureus</i> viable bacteria colonies at single time points and (d) over time. Values are expressed as means and standard deviations, $p < 0.05$ [15].	10
Figure 10: Optical micrographs of the a) Ti-33Nb-3Ga alloy at 5x magnification, b) Ti-33Nb-5Ga alloy at 5x and 20x magnification, c) Ti-6Al-4V reference alloy at 5x and 20x magnification.	18
Figure 11: SEM micrographs of the polished Ti-33Nb-3Ga alloy at magnifications of a) 50x, b) 200x, c) 267x and d) 500x showing distinct β -phase grains.	19
Figure 12: SEM micrographs of the Ti-33Nb-5Ga polished alloy at a) 500x and b) 4000x magnification showing dendritic α -phase colonies, c) 600x and d) 16000x magnification showing transformed martensitic phase, and e) 100x and f) 200x magnification showing equiaxed β -phase grains.	20
Figure 13: SEM micrographs of the reference Ti-6Al-4V polished alloy at magnifications of a) 1000x, b) 5000x, c) 10,000x and d) 20,000x showing alpha equiaxed grains with minor β -phase grains.	20
Figure 14: EDS mapping for the polished alloys, a-d) corresponds to Ti-33Nb-3Ga, e-h) corresponds to Ti-33Nb-5Ga, and i-l) corresponds to the reference Ti-6Al-4V.	21
Figure 15: EDS spectrum analysis of polished samples indicating chemical composition of microstructural features and the overall alloy for a) Ti-33Nb-3Ga, b) Ti-33Nb-5Ga, and c) Ti-6Al-4V.	22
Figure 16: Inverse pole figure (IPF) map of the grains in polished Ti-33Nb-3Ga. Colours correspond to the Miller indices and therefore crystal structure orientations.	23

Figure 17: The mean Vickers microhardness (HV) for the developed alloys and the reference material based on 7 measurements. Errors bars informing standard deviation are provided.....	24
Figure 18: Load-displacement curves from nanoindentation results for a) Ti-33Nb-3Ga, b) Ti-33Nb-5Ga, and c) Ti-6Al-4V.....	24
Figure 19: Young's modulus of the developed alloys and reference material collected by nanoindentation testing over a 4x4 matrix. Errors bars informing standard deviation are provided.....	25
Figure 20: Nanohardness of the developed alloys and reference material collected by nanoindentation testing over a 4x4 matrix. Errors bars informing standard deviation are provided.....	26
Figure 21: Ti-6Al-4V (labelled Ti), Ti-33Nb-3Ga (labelled 3%) and Ti-33Nb-5Ga (labelled 5%) antibacterial activities against Gram-negative <i>Pseudomonas aeruginosa</i> (<i>P. aeruginosa</i>) and Gram-positive <i>Staphylococcus aureus</i> (<i>S. aureus</i>). CLSM pictures and associated plots assessing the antibacterial efficiency of Ti, 3%, and 5% against <i>P. aeruginosa</i> and <i>S. aureus</i> for 6 hours (A) and 24 hours (B). Dead bacteria are red, while living bacteria are green. The scale bar measures 20 μm . $n = 3 \pm \text{SD}$. * $p < 0.1$, ** $p < 0.01$, *** $p < 0.001$, **** $p < 0.0001$	27
Figure 22: Cytocompatibility analysis of the alloys; values are representative of means and standard deviations. The assay showed that no toxic elements were released from the surface of the specimens as there was no significant difference ($p < 0.05$) between the designed alloys and the control after 24 hrs.....	28
Figure 23: Cytoskeleton organisation and cell morphology imaged with an inverted microscope at 200 μm . Images depict stained F-actin (green) and nucleus (blue) for a) Ti-6Al-4V control, b) Ti-33Nb-3Ga, and c) Ti-33Nb-5Ga alloys.....	29
Figure 24: Phase diagram for titanium-niobium alloys [86].	31
Figure 25: Comparison of results collected from microhardness and nanohardness methods for all alloys.....	33

LIST OF TABLES

Table 1: Assessed biocompatibility and biological impacts of various chemical elements, some of which can be incorporated into titanium alloy systems: red, yellow and green indicate serious, moderate and minimal concerns, respectively [23].	3
Table 2: Chemical composition of Ti-33Nb-xGa (x = 3, 5 wt%) alloys in wt%, provided by American Elements.	13
Table 3: Chemical composition of Ti-6Al-4V alloy in wt%, provided by Dynamet.	13
Table 4: The mean microhardness values for each alloy in addition to the reference alloy. Standard deviation is given for each value based on 7 measurements.	23
Table 5: Mean \pm standard deviation of the Young's modulus and nanohardness results for the developed alloys together with the reference material as collected by nanoindentation (4x4 matrix).	25
Table 6: Cytotoxicity assay results, described as means and standard deviations. The p-value is reported, where no significant difference ($p > 0.05$) is observed between alloys.	29

LIST OF PUBLICATIONS

1. McHendrie R., Xiao W., Truong V.K., Hashemi R. Gallium-Containing Materials and their Potential within New-Generation Titanium Alloys for Biomedical Applications. Article currently under review, *Biomimetics* (Impact Factor: 4.5)
2. Development of Novel Ti-33Nb-xGa ($x = 3, 5$ wt%) Alloys with Antibacterial Properties and Low Stiffness for Biomedical Implant Applications. Article in final stage of preparation, to be submitted to *Acta Biomaterialia* (Impact Factor: 9.7)

1.0 INTRODUCTION

The increasing number of implantable medical devices such as orthopaedic implants, owed partly to the prevalence of related health problems and an aging population, has led to an amplified incidence of device-associated infections [1]. The development of implant-related infections, namely biofilms, on the surfaces of implants can result in chronic infections; and hence, implant failure [1]. Having attracted extensive attention as biomedical materials, Titanium (Ti) and its alloys depict a nominal Young's modulus, great strength, and good biocompatibility and corrosion properties [2-5]. This desirable combination of properties has rendered titanium alloys as one of the most suitable biometals for the manufacture of orthopaedic implants such as total hip replacement systems [6-8]. The clinical benchmark among titanium alloys for orthopaedic implant applications is the alpha/beta (α/β) alloy Ti-6Al-4V. However, the disproportionate Young's modulus between Ti-6Al-4V (110 GPa) compared to cortical bone (5-30 GPa) can result in stress-shielding effects which may instigate implant failure and bone resorption [4, 9, 10]. Moreover, it is well reported that Aluminium (Al) and Vanadium (V) can be released from the alloy to elicit serious cytotoxic effects, including neurodivergent diseases and genetic damage [11, 12]. These details have motivated inquiries into Ti-based alloys with a Young's modulus closer to bone, paired with biocompatible alloying elements for biomedical implant applications.

Novel β -type Ti-Nb alloys with non-toxic alloying elements and reduced stiffness levels (Young's moduli) have been the focus of extensive research development in recent years. Despite highly optimised mechanical properties, the major limitations of Ti-Nb alloys include their reduced strength and the prospect of bacterial infection after implantation [4]. Antibacterial effects have previously been demonstrated by the addition of inorganic metallic elements such as Gallium (Ga) to material systems. Ga prevents implant biofilm formation by a mechanism of replacing Iron (Fe) nutrients within bacterial metabolism [13]. This has allowed Ga to be used in the development of biomaterials with antibacterial properties, where even small additions of Ga (1-2 wt%) decreased the biofilm viability of *S. aureus* bacteria by approximately 50% [14, 15]. As a new idea, the addition of Ga to low stiffness Ti-alloys may promote the development of a novel class of biometallic alloys that can offer similar properties to bone, and that could also exhibit antibacterial activity.

This research therefore aims to develop novel β -type Ti-Nb alloys with minor gallium additions that show improved mechanical, antibacterial and cytotoxicity properties to clinical Ti-6Al-4V. The primary aim is to understand how small additions of gallium (3, 5 wt%) affect

the microstructure, mechanical and antibacterial characteristics of a newly developed alloy (Ti-33Nb). This includes to exhibit stiffnesses lower than that of the reference material (Ti-6Al-4V) at 110 GPa, such that alloys are closer in stiffness to bone (5-30 GPa) and stress shielding effects are therefore minimised. Moreover, alloys have been designed with an intended β -phase microstructure, as this phase induces the most desirable mechanical properties. The master alloy should also be designed with no major alloying elements of Al and V due to their inherent cytotoxicity. Furthermore, it is targeted that gallium compositions (wt%) are novel when alloyed to the master alloy. This will allow for the literature gap to be addressed, and the antibacterial effect of Ga to be further clarified within Ti-Nb based systems. In assessing the antibacterial activity and biocompatibility, it is targeted that the alloys depict antimicrobial action with no cytotoxicity. Investigating these research aims will aid in informing the suitability of the developed alloys as orthopaedic implant biomaterials.

The methodology to achieve such aims encompasses various structural, mechanical, and biological methods. This includes the design of novel alloy compositions, followed by their subsequent casting and sample preparation, such as cutting and polishing. Optical Microscopy will be employed to afford optical micrographs of microstructures. Scanning Electron Microscopy (SEM) with Electron Diffraction X-ray Spectroscopy (EDS) will be used to elucidate the microstructures, chemical compositions, and homogeneity of alloys. Mechanical properties will be established from nanoindentation experiments, in addition to Vicker's microhardness investigations. An antimicrobial assay will be conducted to assess the ability of alloys to suppress bacteria and ultimately prevent biofilm formation. Finally, an in-vitro direct cytotoxicity assay will be conducted to evaluate the biocompatibility of the alloys in the presence of human gingival fibroblast cell lines.

This thesis is divided into chapters detailing the introduction, literature review, methodology, results, discussion, conclusion and suggestions for future work. Chapter 1.0 defines the introduction, including project motivations and aims. Chapter 2.0 provides a literature review of related work on new-generation titanium alloys and the addition of gallium to various material systems, while also revealing the literature gap. Methodology in Chapter 3.0 is divided into the alloy composition design, sample fabrication and preparation, microstructural characterisation, mechanical characterisation, and biological characterisation. Chapter 4.0 is dedicated to the results, divided into microstructural characterisation, mechanical characterisation, and biological characterisation. Chapter 5.0 details the discussion and limitations of the results, while Chapter 6.0 is reserved for the conclusion and suggestions for future work.

2.0 LITERATURE REVIEW

New-generation titanium alloys with biocompatible elements and low stiffness levels represent a promising class of materials for use in biomedical implant applications. The addition of gallium alloying elements can impart advantageous properties including antibacterial activity and increased biocompatibility into numerous material systems. These properties underline the promising potential of Ga to mitigate the risk of implant-associated infections and to improve patient outcomes within orthopaedic implant applications. This chapter aims to review the existing literature on new generation β -type titanium alloys in Chapter 2.1, gallium materials in Chapter 2.2, and review of titanium-gallium alloys in Chapter 2.3.

2.1 New generation titanium alloys with biocompatible elements

Numerous studies have been dedicated to the development of titanium alloys with a low Young's modulus comparable to that of cortical bone (5-30 GPa) in addition to the incorporation of biocompatible alloying elements [2, 4, 16-22]. Titanium alloyed with elements such as Zirconium (Zr), Niobium (Nb), Tantalum (Ta), and Tin (Sn) have undergone extensive investigation owing to their superior biocompatibility (Table 1) and promising potential for use in medical applications. This section aims to provide a brief review of β -type titanium alloys with non-toxic alloying elements and reduced stiffness levels.

Table 1: Assessed biocompatibility and biological impacts of various chemical elements, some of which can be incorporated into titanium alloy systems: red, yellow and green indicate serious, moderate and minimal concerns, respectively [23].

Table has been removed in open access version due to Copywrite restrictions.

2.1.1 Influence of alloying elements on microstructure and mechanical properties

In recent years, significant progress has been gained in developing titanium alloy compositions with improved mechanical properties that help resolve the limitations of stress-shielding, and that possess biocompatible elements [10, 24-26]. New generation β -type Ti alloys with biocompatible elements and body-centered cubic (BCC) crystal structures have been the focus of recent developments, as they possess reduced stiffness levels (Young's moduli), which is desirable for implants in contact with bone, and improved wear resistance compared to α and α - β Ti alloys. Among the developed systems, Ti-Nb and its alloys have garnered immense interest due to their desired phase stability, lower Young's modulus (around 65 GPa), and excellent biocompatibility and corrosion resistance [9, 27]. For

example, Tan et al. [28] studied the effect of niobium content on Ti-xNb-7Zr (x = 23, 28, 33 wt%) alloys from a microstructural and mechanical perspective. Employing X-ray diffraction and SEM analysis, it was concluded that the addition of Nb stabilised the β -phase microstructure (Figure 1). By means of nanoindentation methods, the Young's modulus was found to be minimised in the 33Nb wt% alloy composition with a reported value of 29 GPa. These results emphasise that increasing additions of Nb are advantageous, where [27] further elucidated that the minimum modulus for binary Ti-Nb alloys is 65 GPa when Nb alloying additions are approximately 40 wt%. However, while improvements to stiffness was observed, the hardness was largest in the Ti-23Nb-7Zr alloy owing to the sizable α' -phase.

Figure has been removed in open access version due to Copywrite restrictions.

Figure 1: Scanning electron microscopy (SEM) images for (a) Ti-23Nb-7Zr, (b) Ti-28Nb-7Zr, and (c) Ti-33Nb-7Zr at 15,000x magnification [28].

Comparatively, using a combined approach, Mao et al. [29] developed mechanobiologically optimised Ti-35Nb-2Ta-3Zr alloys and analysed their mechanical properties using both conventional tensile tests and finite element models. The alloys exhibited low Young's modulus (47.6 – 53.3 GPa) and greater mechanobiological characteristics compared to conventional Ti-6Al-4V, however, only moderate strength (460 – 577 MPa) was observed [29]. A comparison of the developed alloys to other notable literature is depicted in Figure 2. While benefits to mechanical properties have been observed in literature, a large dissimilarity between the modulus and strength of β -type Ti-Nb alloys to that of bone still exists, which may instigate implant failure. This was observed in investigating β -Ti based Sn alloys Ti-32Nb-(2, 4)Sn [20]. Although a reduction in Young's modulus (64 – 68 GPa) was observed with increasing Sn content, the modulus mismatch persisted, in addition to moderate strength.

Figure has been removed in open access version due to Copywrite restrictions.

Figure 2: Comparison of elastic modulus and UTS of the Ti-35Nb-2Ta-3Zr alloy compared to other alloys developed in literature [29].

2.1.2 Influence of alloying elements on biocompatibility

The fabrication of novel Ti alloys with biocompatible elements and non-cytotoxic effects have been the focus of research in an attempt to extend the longevity of implants, and to improve their success after implantation. Park [30] investigated the biocompatibility of the Ti-13Nb-13Zr alloy using pre-osteoblastic cells and compared the attachment, spreading, viability, activity, and osteoblastic gene expression to Ti-6Al-4V. Compared to the control,

the alloy depicted enriched properties including significantly increased cellular attachment and proliferation [30]. These favourable cell behaviour results were attributed to the use of non-cytotoxic alloying elements. Similarly, Guo et al. [19] studied the biological compatibility of the β -type titanium alloy Ti-35Nb-3Zr-2Ta by corrosion resistance tests and in-vitro experiments to assess the spreading and proliferation of osteoblasts. Although the corrosion resistance was comparable to that of the measured Ti-6Al-4V alloy, osteoblast integration was greatly improved (Figure 3). These results, paired with those of [16, 31, 32] indicate the promising application of these biomaterials for use as modern orthopaedic implants. Though Ti-Nb alloys have emerged as the focus of on-going research into metallic biomaterials, study into the cytocompatibility of promising elements such as Ga has been deficient.

Figure has been removed in open access version due to Copyright restrictions.

Figure 3: The osteoblast viability after 1, 4, 8 and 16 days on samples of Ti-6Al-4V (control) and Ti-35Nb-2Ta-3Zr. Data is expressed as mean \pm standard deviation [19].

2.2 Antibacterial Gallium-based materials

Gallium-based materials have emerged as promising antibacterial agents in inhibiting the activity of numerous bacterial strains, including both Gram-negative and Gram-positive bacteria. Among the developed materials, gallium has been incorporated into bioglasses, liquid metals, and bioceramics. This section aims to review the incorporation of gallium into various materials with a focus on the imparted antibacterial properties.

2.2.1 Gallium in bioglasses

Scaffold materials that contain antibacterial elements have been applied as tissue engineering materials within the body due to their slow release of antibacterial agents. Existing gallium-based drugs often reach the maximum concentration of gallium (III) within a short time, resulting in a negligible antibacterial effect [33]. The sustained release of antibacterial elements is therefore critical to prevent iatrogenic infections, where bioglasses have been employed to achieve slow release of antibacterial agents. Keenan et al. [34] investigated the antibacterial efficiency of bioglass $\text{Si}_2\text{O}-\text{Na}_2\text{O}-\text{CaO}-\text{ZnO}$ using both broth dilution and agar disc diffusion methods. As much as 16 mol% Ga_2O_3 addition to the bioglass was monitored, where inhibition against bacterial strains of *E. coli* and *C. albicans* was observed, however, no inhibition against *S. aureus* was measured [34]. Yielding similar antibacterial results but with a different sample type, Stan et al. [35] examined Ga and Cu doped silica-based bioglasses. Here, the coatings depicted a decrease in magnitude of *S. aureus* by 4 orders after 24 hours (Figure 4).

Figure has been removed in open access version due to Copyright restrictions.

Figure 4: Bacterial survival of *S. aureus* after 24 hrs of (1) seeded colony forming units (CFUs); (2) control sample; (3) bare and silica-rich; (4) SiO₂-CaO-P₂O₅-MgO-CaF₂ sample; (5) Cu and Ga coated SiO₂-CaO-P₂O₅-MgO-CaF₂ substrate [35].

The antimicrobial properties of gallium when incorporated into borate and phosphate glasses have also been demonstrated. The sustained release of gallium from the B₂O₃-Na₂O-CaO-P₂O₅-ZnO glass system was observed over 28 days using the agar disc diffusion method [36]. Higher antibacterial effects against *P. aeruginosa* were observed with increasing concentrations of gallium [36]. Other studies [37] [38] with comparable compositions have also demonstrated bacterial inhibition from gallium addition. By employing a different approach to [36], Valappil et al. [39] reported the effect of Ga-doped phosphate-based bioglasses via a disk diffusion assay. Even 1 mol% of Ga addition was sufficient to cause a potent antibacterial effect by considerably inhibiting biofilm formation (Figure 5). Additional evidence of inhibition against these bacterial strains within phosphate glasses paired with gallium in 1 and 3 mol% has been demonstrated in [40, 41]. Furthermore, in a recent study by Pourshahrestani et al. [42], the antibacterial effect of sol-gel-derived 1-3 mol% Ga₂O₃ bioactive glasses 80SiO₂-15CaO-5P₂O₅ (mol%) was investigated via an evaporation-induced self-assembly process. It was shown that the addition of 3 mol% Ga₂O₃ yielded the greatest antibacterial effect against *S. aureus* with 99% after 12 hrs of incubation, where all samples exerted an antibacterial effect against *E. coli* and *S. aureus*. Though the potent antibacterial effect of gallium-incorporated bioglasses against numerous bacterial strains has been reported, there exists evidence in literature of Ga³⁺ being unable to be released from the glass network of bioglass samples to the surrounding medium. Studying the same sol-gel-derived bioglass matrix as [42], Salinas and Vallet-Regi [43] found that 3.5 mol% Ga₂O₃ substitution for SiO₂ resulted in negligible release of Ga³⁺ ions from the glass network. It was concluded that the sample therefore likely imparted no antibacterial property to the glasses. This demonstrates the necessity for further research into gallium's antimicrobial mechanism, particularly within a range of samples.

Figure has been removed in open access version due to Copyright restrictions.

Figure 5: a) Results of Ga₂O₃-doped phosphate-based glasses in 0, 1, 3 and 5 mol % using a disc diffusion assay against *S. aureus*, *E. coli*, *P. aeruginosa*, methicillin-resistant *S. aureus*, and *C. difficile*. b) The viability of *P. aeruginosa* from 0, 1, and 3 mol % Ga₂O₃-doped phosphate-based glasses after 4, 12 and 24 hrs [39].

2.2.2 Gallium in liquid metals

Liquid metals (LMs) represent an emerging metallic material in research due to their excellent biocompatibility, metallic properties, and flexibility. LMs show attractive results when applied to biomedical therapeutics, where gallium addition has been demonstrated for its promising antimicrobial action. For instance, novel composite coatings created with hydroxyapatite (HAp) and gallium liquid metal (LM) through atmospheric plasma spray (APS) exhibited impressive antibacterial effectiveness against initial attachments and established biofilms of *S. aureus* and *P. aeruginosa*, both at 18 hours and after 7 days. [44]. In the work of Li et al. [45], Ga^{3+} released from EGaIn was found to trigger the formation of reactive oxygen species, resulting in bacterial cell death [45]. Furthermore, LM nanodroplets were found to have strong adhesion on bacterial and fungal cell surfaces, leading to membrane disruption [46]. The same research group further developed the LM-textiles to inhibit the growth of both pathogenic *S. aureus* and *P. aeruginosa* [47]. In the work of [48], their results also showed the antibacterial and antibiofilm activity of magneto-responsive gallium-based LM droplets after magnetic activation. Assessment against both Gram-negative and Gram-positive biofilms revealed that more than 99% of bacteria became nonviable after 90 minutes, where biofilms were permanently destroyed (Figure 6). Similar efficacies have also been demonstrated within LM-polymer composite films, where He et al. [49] prepared an antimicrobial and self-healing sample by combining LM nanodroplets with polydimethylsiloxane (PDMS). *S. aureus* and *E. coli* bacteria were removed by over 90% and was attributed to Ga atom exposure.

Figure has been removed in open access version due to Copywrite restrictions.

Figure 6: Control and magnetically activated (treated) gallium-based LM against *P. aeruginosa* and *S. aureus*: (A) Raw colony-forming unit (CFU), and (B) logarithmic CFU depiction [48].

2.2.3 Gallium in bioceramic systems

As the functionalisation of biomaterials receives greater interest for the modulation of modern health issues, bioceramics, with a focus on calcium phosphate (CaP) materials, represent a leading material within this area. These materials have been the subject of research with a focus on their bone regeneration properties and in facilitating bone cell turnover [50]. Although there is a scarcity of research into antibacterial CaPs, gallium has been employed within some studies for its potent antibacterial effect. Kurtjak et al. [51, 52] incorporated Ga into hydroxyapatite (HAp) to afford the HAp(Ga) sample. By means of the disc diffusion method, clean inhibition zones against *P. aeruginosa* were afforded after 24 hours and were attributed to gallium's bactericidal action. Though the (HAp(Ga)(TR))

material depicted excellent antibacterial activity, the sample (HAp(Ga)(IE)) produced by the ion exchange method depicted superior inhibition of *P. aeruginosa* bacteria. This difference is mostly attributed to the fast ion release. In a later study [53], however, HAp(Ga) functionalised with gold nanoparticles depicted inhibition against *E. coli*, *S. aureus*, and *S. epidermidis*, while the non-functionalised HAp(Ga) demonstrated no antibacterial activity. Indeed, recent research has demonstrated the antibacterial activity of Ga incorporated CaPs, but their cytotoxicity remains questionable. Using the same methods, [51] and [52] used human and animal fibroblasts to evaluate the cytotoxicity of HAp(Ga) in-vitro. At concentrations of HAp(Ga) less than or equal to the minimal inhibition concentration (MIC), cell viability was approximately 80%. However, both studies indicated that once the MIC was exceeded, the viability of human fibroblasts decreased to 50%. This indicates the sensitivity of these compounds and the necessity to monitor their potential toxic effects on cell viability.

2.3 Titanium-Gallium based systems

The integration of gallium into titanium-based materials, namely new generation β -type alloys, has demonstrated desirable antimicrobial activity, biocompatibility, and improved mechanical properties and microstructures. Ti-Ga based materials, including coatings, nanomaterials, and alloys, are reviewed based on such properties, with a focus on their suitability for orthopaedic implant applications. The materials that have incorporated gallium coatings onto titanium substrates reported in literature are summarised in Appendix A, Table A.1, where Appendix A Table A.2 summarises various Ti-Ga based alloys found in literature.

2.3.1 Titanium-Gallium coatings

The inability of Ti alloys to prevent the onset of bacterial infection after orthopaedic medical device implantation is among the major features affecting their efficacy within biomedical applications. It is clinically imperative to prevent the formation of biofilms as infections raise morbidity and mortality rates, which can double following revision surgeries [54]. Various studies have documented that Ti alloys doped or alloyed with elements that exhibit an antibacterial activity, such as gallium, depict resistance against biofilm formation and bacterial growth [3, 9, 14, 15, 54-61]. For instance, in developing next generation implant coatings, Stuart et al. [55, 62] incorporated gallium into phosphate bioactive glasses (PBG) that were subsequently applied to commercially pure titanium. Antibacterial assays depicted that the Ga-PBG coatings reduced the viability of *S. aureus* and *E. coli* bacteria, while in-vitro cytotoxicity tests on human fibroblast cells indicated good cytocompatibilities. In addition, nanoindentation methods were employed to characterise their mechanical

properties, which has only been considered elsewhere in literature for Ga-coated Ti materials by [15]. The stiffness was reported between the ranges of 65.3 – 77.6 GPa, and the hardness values between 4.7 – 7.4 GPa, where increasing gallium addition improved the mechanical properties. Studying the antibacterial activity and biocompatibility of a similar sample, Yamaguchi et al. [56] explored the antibacterial activity of gallium-incorporated calcium titanate (CT) and gallium titanate (GCT) coated to titanium metal. It highlighted the high antibacterial activity possessed by the material towards *A. baumannii* and the improved bioactivity (Figure 7). Similarly, other surface coatings have also been applied to 3D printed titanium implants which exhibited comparable results [63].

Figure has been removed in open access version due to Copywrite restrictions.

Figure 7: The live/dead biofilm biomass (%) of *A. baumannii* after 7 days from (a) control Ti, (b) Ti with Ga-containing calcium titanate, and (c) Ti with gallium titanate (GT) [56].

To Ti-based implants, Li et al. [58] synthesised a layered double hydroxide (LDH) film composed of strontium and gallium ions by hydrothermal methods. Inhibition of *E. coli* and *S. aureus* were observed and was owed to Ga^{3+} action against bacterial metabolism. Also using a hydrothermal method, Qiao et al. [59] developed titanium surface-functionalised SrTiO_3 nanotubes coated with a layer of polydopamine and gallium nitrate. The antibacterial assay depicted that gallium coated samples prevented bacterial colony formation of *S. aureus* and *E. coli* with enhanced antimicrobial action. Notably, after 24 hours, almost no bacteria remained, where the substrates did not exhibit a reduction in antibacterial activity until after 7 days, where 72% of antibacterial action was retained for as much as 14 days [59]. Although gallium has definite antibacterial effects, this study highlighted its difficulty in releasing adequate quantities of Ga^{3+} over lasting conditions. This effect is owed to gallium being almost completely hydrolysed under physiological conditions. In assessing the cytocompatibilities of a similar sample to that of [59], Chen et al. [64] fabricated a number of Mg-Ga LDH nanosheets on alkali-heat-treated titanium implants. The Mg/Ga coated titanium implants exhibited promoted osteogenesis and suppressed osteoclast generation – indicating superior cytocompatibilities.

With a focus on improving the performance of dental implants and other biomedical materials, Cochis et al. [61] investigated the efficacy of gallium-coated titanium surfaces using the anodic spark plasma (ASD) surface modification technique. In-vivo antibacterial assays on the dental implant revealed the efficacy of the gallium-coated sample compared to the silver-coated sample, where a strong inhibition of 27-35% against metabolic activity was observed [61]. In a later study by Cochis et al. [14], the authors further investigated the

effectiveness of the same samples against multidrug-resistant *A. baumannii*. Again, the Ga-doped Ti sample exhibited stronger bacterial inhibition against various strains of *A. baumannii* compared to that of Ag-doped Ti, with no cytotoxic effect [14]. Gallium therefore imparted a crucial role in discouraging the colonisation and growth of *A. baumannii* on the surface of the implant due to its gradual release from the coating (Figure 8). Importantly, no detrimental impact to the mechanical properties were observed with the addition of gallium to the titanium scaffolds. However, the evaluation of mechanical properties did not receive extensive analysis, where properties also did not differ significantly from the Ti control. Further research is therefore warranted to comprehensively elucidate the effect of gallium on the mechanical properties of titanium alloy systems.

Figure has been removed in open access version due to Copyright restrictions.

Figure 8: Release of antibacterial activity against *A. baumannii* measured over 21 days (a) Silver release from AgCis and AgNPS (b) gallium release from GaCis and GaOss [14].

2.3.2 Titanium-Gallium based alloys

Metal alloys are frequently employed as clinical orthopaedic implants, where the addition of alloying elements such as gallium can prevent implant biofilm formation and bactericidal activity. Cochis et al. [15] metallurgically added gallium (1, 2, 20 wt%) to the titanium alloy Ti-Al-Zr-Si and reported the successful inhibition of *S. aureus* bacteria, with more than 80% reduction in the metabolic activity of the bacterial strain compared to the control sample, as shown in Figure 9. Promisingly, even 1-2 wt% additions of Ga to Ti-Al-Zr-Si alloys depicted potent antibacterial efficiency [15]. Although samples ensured release of Ga^{3+} ions and strong antibacterial effects, this efficacy was only observed for at least 3 days. In addition to the antibacterial effect, the cytocompatibility was analysed by both direct and indirect assays with mature osteoblast and preosteoblast cells where great cytocompatibility was revealed. Though mechanical properties were not investigated, it is predicted that greater concentrations of gallium additions would compromise the mechanical properties, as gallium is an α -phase stabiliser and should therefore be kept low when alloyed [15].

Figure has been removed in open access version due to Copyright restrictions.

Figure 9: Antibacterial effect of the Ti-8Al-3Si-3Zr-(1, 2, 20 wt%)-Ga alloys and control samples: (a) metabolic activity at 24, 48, 72 h of *S. aureus*, (b) metabolic activity over time of *S. aureus*, (c) *S. aureus* viable bacteria colonies at single time points and (d) over time. Values are expressed as means and standard deviations, $p < 0.05$ [15].

Indeed, alloying of Ga to Ti-Nb alloys and its effect on transformation temperature properties have been investigated, but its influence on the mechanical behaviour was not

investigated until Alberta et al. [9, 65, 66]. In investigating Ti-45Nb-xGa ($x = 2, 4, 6, 8$ wt%) alloys, it was revealed that the master alloy paired with 4 wt% Ga depicted the best mechanical properties. This included a near 40% increase in strength over Ti-45Nb [9]. By tensile and microhardness tests, increasing additions of gallium improved the strength of the alloys, with the maximum yield strength and microhardness being 620 ± 2 MPa and 232 ± 5 HV, respectively [9]. The same trends were observed for the Young's modulus and ductility, with values in the range of $73 \div 82$ GPa for stiffness, and a maximum ductility of 32% [9]. Therefore, the addition of gallium to Ti-45Nb alloys affords a desirable balance between low Young's modulus and increased strength. In another study, the same authors also investigated the influence of both Ga and Cu to the corrosion characteristics, phase constitution and mechanical properties when alloyed to Ti-45Nb [65]. Using simulated body fluids to assess the corrosion characteristics, no deleterious effect on the corrosion resistance was observed with the addition of Ga. Excellent plasticity was detected and attributed to work hardening, where similar tensile strengths and Young's modulus results were founded to that of the initial study. However, the antibacterial and cytotoxic effect of gallium additions to Ti-Nb alloys is yet to be studied and exhibits a large gap within the literature.

3.0 METHODOLOGY

3.1 Alloy Composition Design

The compositions of novel new-generation titanium alloys were designed based on extensive evaluation of Ti-Nb β -phase alloys reported within the literature, as shown in Appendix B. New-generation Ti alloys have received widespread interest, where the Ti-Nb system and its alloys show among the most promising properties. This includes desired phase morphology, reduced Young's modulus, corrosion resistance, and excellent biocompatibilities [2, 9, 16, 21, 28, 65-68]. This underpins the reasoning for its incorporation into the master alloy. The content of niobium within the master alloy was intentionally selected as 33 wt%, as Nb content above 30 wt% promotes a single bcc β -phase [69]. This microstructure is known to optimise mechanical properties, including to reduce the Young's modulus [66]. Hanada et al. [27] reported that the minimum modulus for binary Ti-Nb alloys is 65 GPa when Nb alloying additions are approximately 40 wt%, however, greater α' phase was exhibited which can be deleterious to the Young's modulus. This indicates that niobium content should be kept within the range of 30 to 40 wt% to exhibit optimised mechanical properties. Furthermore, Tan et al. [28] investigated the effect of increased elemental niobium content on the microstructural and mechanical properties of Ti-xNb-7Zr (x = 23, 28, 33 wt%) alloys. The Young's modulus was minimised in the 33 wt% Nb alloy at 29.0 GPa. Through consideration of all rationales, the niobium content was therefore selected as 33 wt% within the master alloy.

The incorporation of minor alloying additions of gallium to the Ti-33Nb master alloy, at concentrations of 3 and 5 wt%, represent novelty in the literature. Compositions were systematically chosen based on the antibacterial effect of Ga seen for 1-2 wt% additions [15], and because Ga is an α -phase stabiliser and should therefore be kept low when alloyed. Alberta et al. [9] also found that between 2, 4, 6 and 8 wt% incorporations of gallium, the 4 wt% alloy showed the best combination of mechanical properties [66]. Based on these reasonings, novel alloying additions of 3 and 5 wt% Ga to the Ti-33Nb master alloy were designed, therefore affording Ti-33Nb-3Ga and Ti-33Nb-5Ga.

3.2 Sample Fabrication & Preparation

3.2.1 Alloy Casting

Alloys of composition Ti-33Nb-xGa (x = 3, 5 wt%, chemical composition provided in Table 2) were produced as cylindrical rods (diameter = 20 mm and thickness = 40 mm) by

American Elements (Los Angeles, CA, USA) using an arc melting furnace under argon atmosphere with high purity Ti, Nb, and Ga pieces. The alloys were subsequently cast as cylindrical rods in a cold crucible, and subject to post treatment homogenisation processes. In the present study, the developed alloys were compared to the standard Ti-6Al-4V alloy, produced by Dynamet (Wyomissing, PA, USA), of chemical composition specified in Table 3.

Table 2: Chemical composition of Ti-33Nb-xGa (x = 3, 5 wt%) alloys in wt%, provided by American Elements.

Alloy	Elemental Composition (wt%)		
	Ti	Nb	Ga
Ti-33Nb-3Ga	63.9968	32.9835	2.9997
Ti-33Nb-5Ga	61.9969	32.9835	4.9995

Table 3: Chemical composition of Ti-6Al-4V alloy in wt%, provided by Dynamet.

Alloy	Elemental Composition (wt%)		
	Ti	Al	V
Ti-6Al-4V	89.8030	6.0000	4.0050

3.2.2 Sample Preparation

Alloy samples were sectioned using a precision saw equipped with a diamond blade into 20 mm by 8 mm thickness disks. The samples were subsequently mounted in cold-hardening resin by homogenisation of liquid Versocit 2 (10 g) in Versocit 2 powder (20 g) followed by curing for 10 min. Mounted samples were mechanically ground using a Tegramin 25 polishing machine with resin bonded diamonds in a rigid disc (MD-Meso). Plane grinding was followed by the single fine grinding step, using MD-Largo paired with abrasive 9 μm diamond suspension. Subsequently, chemical-mechanical polishing was conducted using a mixture of colloidal silica (OP-S) and hydrogen peroxide (10-30%) with MD-Chem polishing disks. The reaction product generated between hydrogen peroxide and titanium is continuously removed from the surface of the alloy samples by the silica suspension, resulting in a surface free of mechanical deformation. Additional details related to the grinding and polishing steps are depicted in Appendix C. Finally, samples were cleaned in an ultrasonic bath (5 min) and dried with condensed air. The fabricated alloys were referenced to Ti-6Al-4V, which was subject to the same sample preparation methods.

3.3 Microstructural Characterisation

3.3.1 Optical Microscopy

Microstructures of the polished samples were observed using a Zeiss Axio Imager Z2 optical microscope under illumination with white light. Samples for optical microscopy were sectioned from the as-cast alloys and polished to a mirror-like finish, as described in Section 3.2.2. Sample collection was performed at Flinders University (Adelaide, SA, Australia). Objective lenses ranging from 5 to 50x magnification were used for imaging each sample, where a Zeiss AxioCam 305 colour camera was used to record the microstructures. Camera acquisition settings were adjusted prior to image collection.

3.3.2 SEM and EDS

The microstructures of the developed alloys were analysed by means of a Scanning Electron Microscope used by Flinders Microscopy and Microanalysis (Adelaide, SA, Australia), with an FEI Inspect F50 SEM equipped with an EDT secondary electron detector, concentric backscatter electron detector and Ametek EDAX EDS detector. Samples for SEM analysis were cut from the as-cast alloys, mechanically ground, and polished, as described in Section 3.2.2. SEM images were scanned at a height of 10 mm, an emission current of 178.3 μA , and a voltage of 20 kV.

3.4 Mechanical Characterisation

3.4.1 Microhardness

Microhardness testing was conducted on polished, unembedded samples using a Vickers microhardness tester (Struers DuraScan-20) paired with a diamond pyramid indenter at Flinders University (Adelaide, SA, Australia). Each sample was subject to 7 measurements within a matrix at an established load of 5 HV (49.04 N) and a dwell time of 3 s.

3.4.2 Nanoindentation

Given the size limitations of the as-cast samples, nanoindentation testing was performed to elucidate the mechanical properties of the alloys, as tensile testing requires large, dog-bone alloy morphologies. Nanoindentation is a well-established method that has been used extensively in the existing literature, which attests to its reliability and relevance for this research. Nanoindentation testing was performed using an IBIS Nanoindentation System coupled with a Berkovich diamond indenter at Adelaide Microscopy (Adelaide, SA, Australia). The polished samples each received 16 measurements in a rectangular map

(4x4), where the indentations were distanced by 15 μm to prevent the influence of residual strain between adjacent indentations. The applied load was kept constant at 100 mN, with a depth of 19.2 μm , and a working distance of approximately 65 μm . Measurements were taken in accordance with ISO 14577-1, including a contact force 10% of the maximum at an unloading rate of 2.5 mN/second. The IBIS nanoindentation software automatically processes results, however, the mechanical properties may be calculated from the theoretical framework developed in Equation 1 and 2 for Young's modulus, as well as Equation 3 for hardness.

$$E_r = \frac{\sqrt{\pi}S}{2\sqrt{A}} \quad (1)$$

$$\frac{1}{E_r} = \frac{(1 - \nu^2)}{E} + \frac{(1 - \nu_i^2)}{E_i} \quad (2)$$

$$H = \frac{P_{max}}{A} \quad (3)$$

where E_r is the reduced modulus, S is the unloading stiffness, and A is the contact area. E and ν represent the Young's modulus and Poisson's ratio of the material respectively, and E_i and ν_i signify the same parameters but for the indenter. The hardness, H , is expressed as the maximum load P_{max} per the area A of indentation under the specified load.

3.5 Biological Characterisation

3.5.1 Antimicrobial Activity Assay

Staphylococcus aureus (*S. aureus*) ATCC 25923 and *Pseudomonas aeruginosa* (*P. aeruginosa*) ATCC 15692 were obtained from glycerol stocks maintained at a temperature of -80 °C. A loop-full of the stock bacteria was thereafter placed onto a Tryptic Soy Broth (TSB) agar plate and incubated overnight. On a subsequent day, a single colony was placed into a Tryptic Soy Broth (TSB) medium for further incubation overnight. The cell density was measured using a spectrophotometer at a wavelength of 600 nm. All methodology was performed at Flinders University Health and Medical Sciences (Adelaide, SA, Australia).

The specimens were sectioned into 10 mm diameter and 3 mm thickness profiles using a diamond saw and were subsequently subjected to a 5-min ultrasonic cleaning process. The specimens, labelled as Ti, 3%, and 5%, were carefully placed in a 24-well plate. Each well of the plate contained 500 μL of bacterial suspension with a concentration of 10^6 CFU mL^{-1} in TSB, where specimens were positioned such that they were fully submerged in

solution. Specimens were incubated at 37 °C for 6 and 18 hrs in a humidified chamber. Subsequently, the samples underwent three rinses with phosphate-buffered saline (PBS) and were transferred to a fresh 24-well plate. In this experiment, a volume of 1 mL of BacLight Live/Dead stain (Invitrogen, ThermoFisher, MA, USA) was added to each well. The stain is composed of an equal mixture of Syto9 and Propidium Iodide (PI), resulting in a final concentration of 1.5 $\mu\text{L mL}^{-1}$ in PBS. After a 15-minute period of incubation in a dark environment at room temperature, fast imaging was performed using a Zeiss_LSM880 Confocal laser scanning microscope (Oberkochen, Germany). The emission and excitation spectra for PI and Syto9 were configured at wavelengths of 490/635 nm and 480/500 nm, respectively. The viable-to-non-viable cell ratio was quantified using ImageJ Fiji software (version 1.53a). Antibacterial efficacy was calculated from the formula in Equation 4.

$$\text{Antibacterial percentage} = \frac{\text{Dead bacteria}}{\text{Total bacteria}} \times 100\% \quad (4)$$

3.5.2 Cytotoxicity Assay

The in-vitro cytocompatibility evaluation of Ti-33Nb-3Ga, Ti-33Nb-5Ga, and control Ti-6Al-4V alloys was performed using direct methods on the human gingival fibroblast cell line (hGF) at Flinders University Health and Medical Sciences (Adelaide, SA, Australia). The sectioned pieces (10 x 3 mm) were sterilised within 80% ethanol for 15 min and rinsed three times with PBS. Cells were cultured in Dulbecco's modified Eagles medium (DMEM/F-12 GlutaMAX supplement; ThermoFisher, MA, USA), 10 vol% fetal bovine solution (FBS), and 1 vol% of penicillin-streptomycin (ThermoFisher, MA, USA), which will hereby be referred to as the medium. For the direct cell assay, hGF was washed with PBS, and hGF differentiated macrophages were detached with trypsin (0.25 vol%) in a 37 °C humidified incubator with 5% CO₂ for 2 min. To neutralise the trypsin, medium was added (3 mL), collected into a sterilised tube (15 mL), and centrifuged (1000 rpm, 2 min), where the supernatant was subsequently removed, and the pellets resuspended in fresh medium (2 mL). From this suspension, 10 μL was mixed with 10 μL of trypan blue solution (ThermoFisher, MA, USA) and was evaluated using an automated cell counter (Invitrogen Countless 3 Automated Cell Counter) to contain 1×10^6 cells per 1 mL. The material discs were placed in a 24 well plate and seeded with hGF at a density of 440,000 cells/mL. After 24 hrs of direct cell contact in a 37 °C humidified incubator with 5% CO₂, 10 vol% MTT solution (3-(4,5-dimethylthiazol-2-yl)-2,5-diphenyl tetrazolium bromide) was introduced and incubated for 2 hrs. The supernatants were then discarded, DMSO added, and shaken for 5 min. The absorbance of

the samples was measured in a 96 well plate at a wavelength of 570 nm using an MTT colorimetric assay to quantify the number of viable cells adhered to the surface.

3.5.2.1 F-actin Staining

Cells were grown in a 24-well plate (40,000 cells/well) with material, and subsequently incubated for 24 hrs in a 37 °C humidified incubator with 5% CO₂. Samples were washed twice with pre-warmed PBS, and materials were fixed with paraformaldehyde solution (3.7%) for 15 min, followed by additional PBS washing. Triton X-100 (0.1%) in PBS was introduced to the fixed cells for 3-5 min to increase permeability and subsequently washed with PBS two times. A phalloidin-conjugate working solution was prepared and added, followed by incubation at room temperature for 40 min, and additional PBS washing. The mounting of specimens with DAPI (aqueous, fluoroshield ab104139) and mounting medium was conducted, where specimens were imaged using an Olympus IX83 Inverted Microscope.

3.5.3 Statistical Analysis

Antibacterial activity and cytotoxicity assay results are expressed as means \pm standard deviations. Statistical analyses were performed using Student's t-test. Differences were considered statistically significant at $p < 0.05$.

4.0 RESULTS

4.1 Microstructural Characterisation

4.1.1 Optical Microscopy

The microstructures obtained for polished Ti-33Nb-3Ga, Ti-33Nb-5Ga, and Ti-6Al-4V alloys by optical microscopy are depicted in Figure 10a-c. Figure 10a shows the optical micrographs of the 3 wt% Ga alloy, which consists of equiaxed β -grains in varying grain sizes ranging from 300 to 800 μm . Comparatively, the microstructure of Ti-33Nb-5Ga in Figure 10b depicts α -phase dendritic branches encapsulated in β -phase equiaxed grains and grain boundaries, with the average grain size ranging from 100 to 400 μm . Furthermore, the microstructure of the Ti-6Al-4V reference alloy depicts homogenous grain distribution. However, due to such homogeneity, optical microscopy failed to observe distinctive microstructural features at varying magnifications. Pores and surface contaminants are observable across the morphologies of all alloys, including carbon deposits. Results are highly reproducible due to the polishing method.

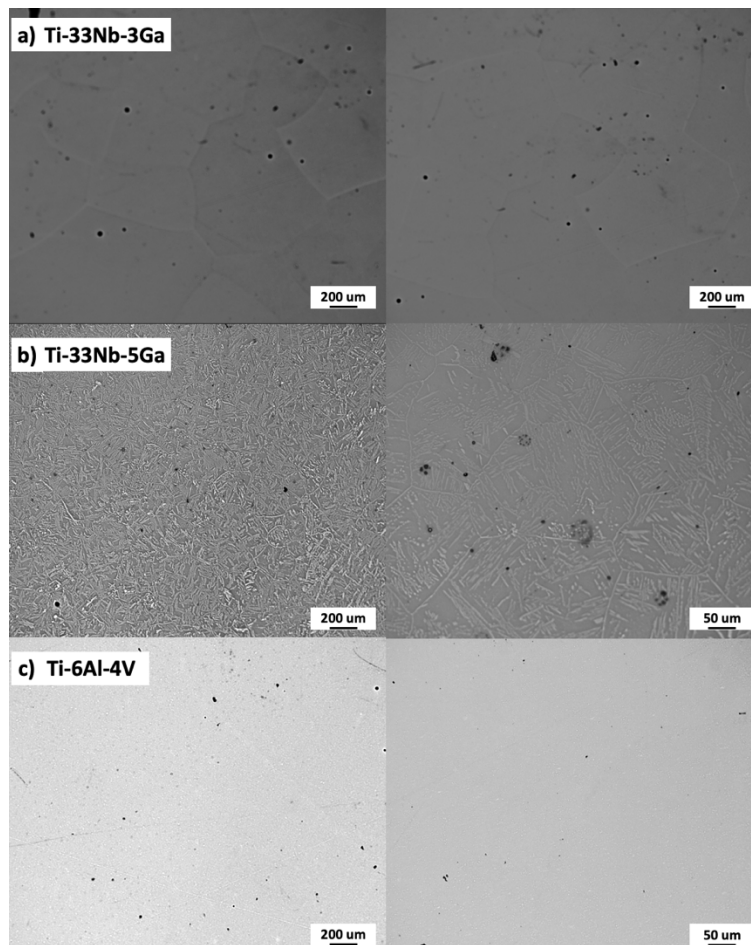


Figure 10: Optical micrographs of the a) Ti-33Nb-3Ga alloy at 5x magnification, b) Ti-33Nb-5Ga alloy at 5x and 20x magnification, c) Ti-6Al-4V reference alloy at 5x and 20x magnification.

4.1.2 SEM and EDS

The microstructures of Ti-33Nb-3Ga and Ti-33Nb-5Ga, together with the reference Ti-6Al-4V alloy, observed by SEM imaging is depicted in Figure 11, Figure 12, and Figure 13 respectively. Each of the developed alloys show dissimilar microstructures due to differing elemental compositions of gallium (wt%). SEM backscattered micrographs for the Ti-33Nb-3Ga alloy, shown in Figure 11a-d, depict a single-phase character consisting of equiaxed β -grains with grain sizes in the range of approximately 400 to 900 μm . Figure 12a-f illustrates the SEM backscattered micrographs for the Ti-33Nb-5Ga alloy, which consists of various phases dominated by dendritic and inter-dendritic regions (Figure 12a-b). High contrast, dendritic regions are evidence of α -phase colonies ranging from 3 to 6 μm , while lighter regions correspond to a β -phase equiaxed matrix. Grain boundaries are enriched in α -phase character for Ti-33Nb-5Ga, shown in Figure 12a,c. Martensitic transformation of the β -phase into α'' -phase is also observed (Figure 12c-d). Moreover, single-phase β -type character is depicted in Figure 12e-f, which is comparable to the microstructure observed for the 3 wt% Ga sample. Grain sizes in the 5 wt% Ga alloy appear to diminish compared to the 3 wt% Ga alloy, with an average grain size of 500 μm . SEM images of the reference alloy depict uniform phase distribution with mostly homogenous grain sizes ranging from 1 to 4 μm , as observed in Figure 13a-d. The Ti-6Al-4V microstructure contains primary alpha equiaxed grains with transformed beta grains uniformly distributed in the alpha matrix. Shown in Figure 13d, the presence of transformed beta grains consisting of elongated alpha needles is additionally observed.

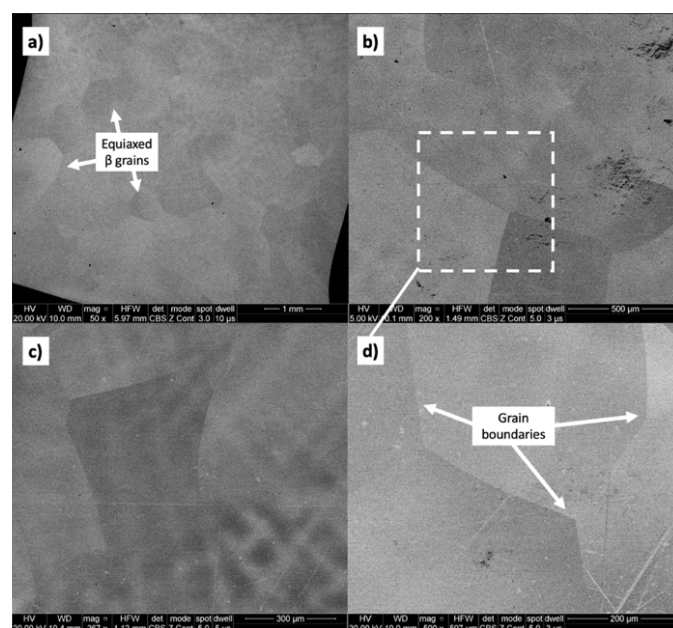


Figure 11: SEM micrographs of the polished Ti-33Nb-3Ga alloy at magnifications of a) 50x, b) 200x, c) 267x and d) 500x showing distinct β -phase grains.

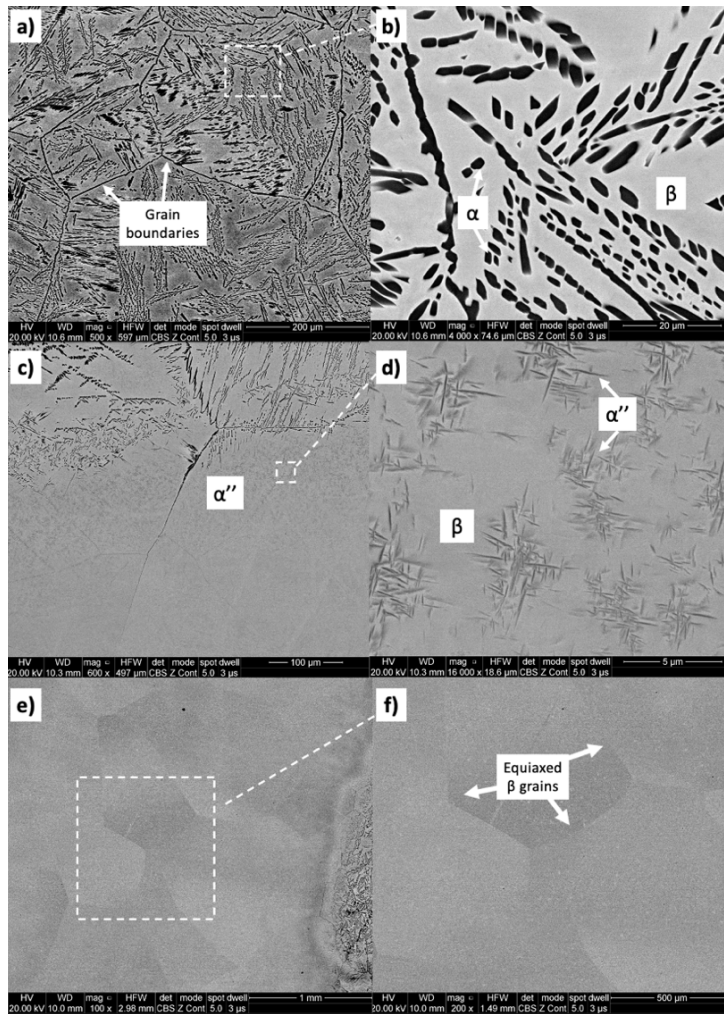


Figure 12: SEM micrographs of the Ti-33Nb-5Ga polished alloy at a) 500x and b) 4000x magnification showing dendritic α -phase colonies, c) 600x and d) 16000x magnification showing transformed martensitic phase, and e) 100x and f) 200x magnification showing equiaxed β -phase grains.

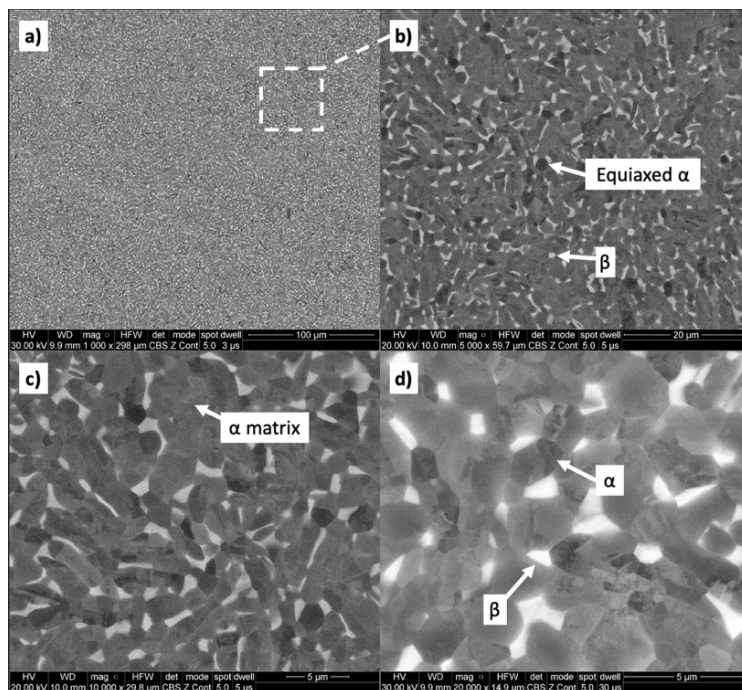


Figure 13: SEM micrographs of the reference Ti-6Al-4V polished alloy at magnifications of a) 1000x, b) 5000x, c) 10,000x and d) 20,000x showing alpha equiaxed grains with minor β -phase grains.

The results from EDS analysis aid in elucidating the chemical composition and homogeneity of the developed alloys, as shown in Figure 14 and Figure 15. Elemental mappings of the Ti-33Nb-3Ga alloy reveal the presence of a chemically homogenous microstructure, depicted in Figure 14a-d. Such uniformity is also corroborated by the results in Figure 15a, where lighter and darker grains correspond to the same elemental composition. The 5 wt% Ga alloy demonstrates elementally enriched areas within the microstructure, shown by the EDS mapping in Figure 14e-h. Corroborating with this result, Figure 15b reveals that the darker, α -phase regions are enriched with titanium, while the β -phase is more elementally concentrated in both niobium and gallium. Furthermore, the Ti-6Al-4V reference alloy depicted a chemically homogenous microstructure from the elemental mappings in Figure 14i-l. Chemical composition analysis in Figure 15c further discloses the micrometric homogenous distribution of alloying elements among grains within this alloy. Revealed by EDS, the chemical composition reported for the 3 wt% alloy was 67.73 wt% Ti, 27.48 wt% Nb, and 4.80 wt% Ga, while the chemical composition of the 5 wt% alloy was indicated as 70.16 wt% Ti, 27.44 wt% Nb, and 2.40 wt% Ga. However, it is widely acknowledged that this method does not yield precise chemical composition analysis, where the results should be considered as indicative rather than definitive.

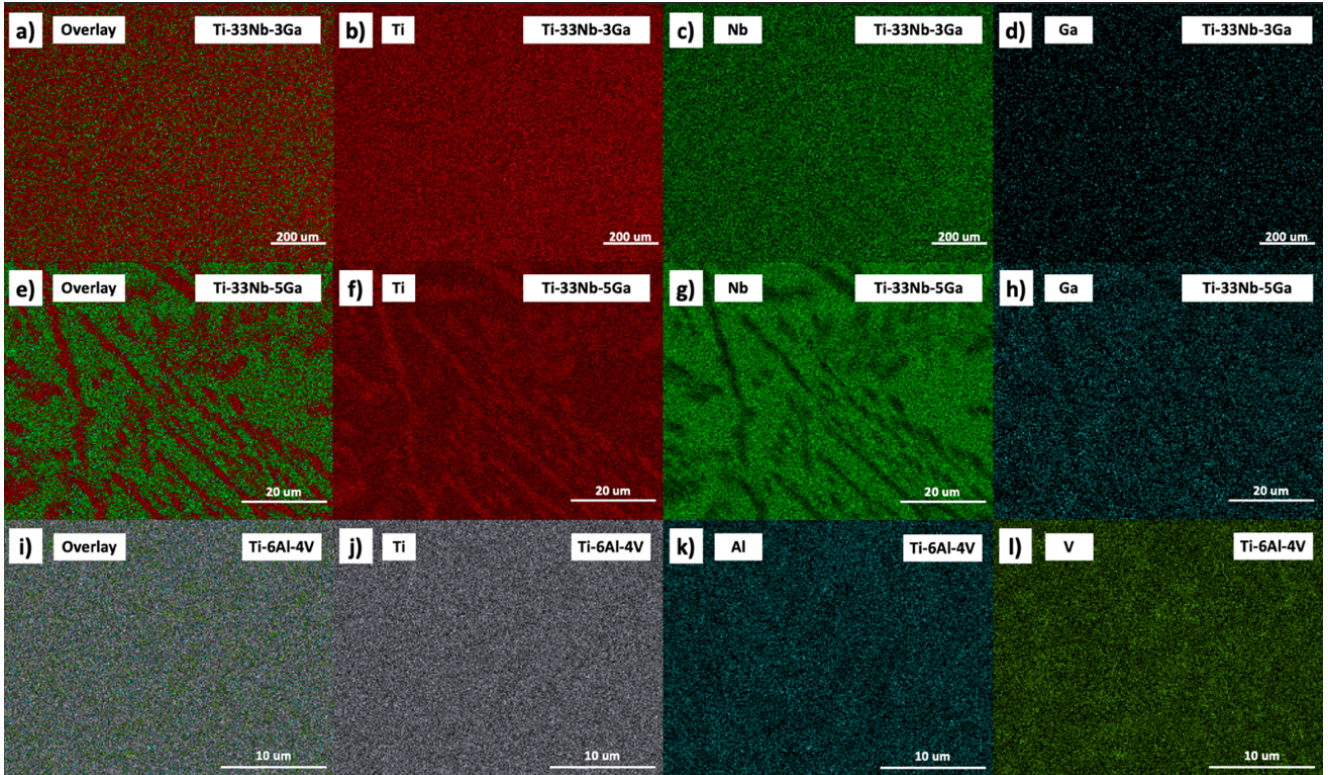


Figure 14: EDS mapping for the polished alloys, a-d) corresponds to Ti-33Nb-3Ga, e-h) corresponds to Ti-33Nb-5Ga, and i-l) corresponds to the reference Ti-6Al-4V.

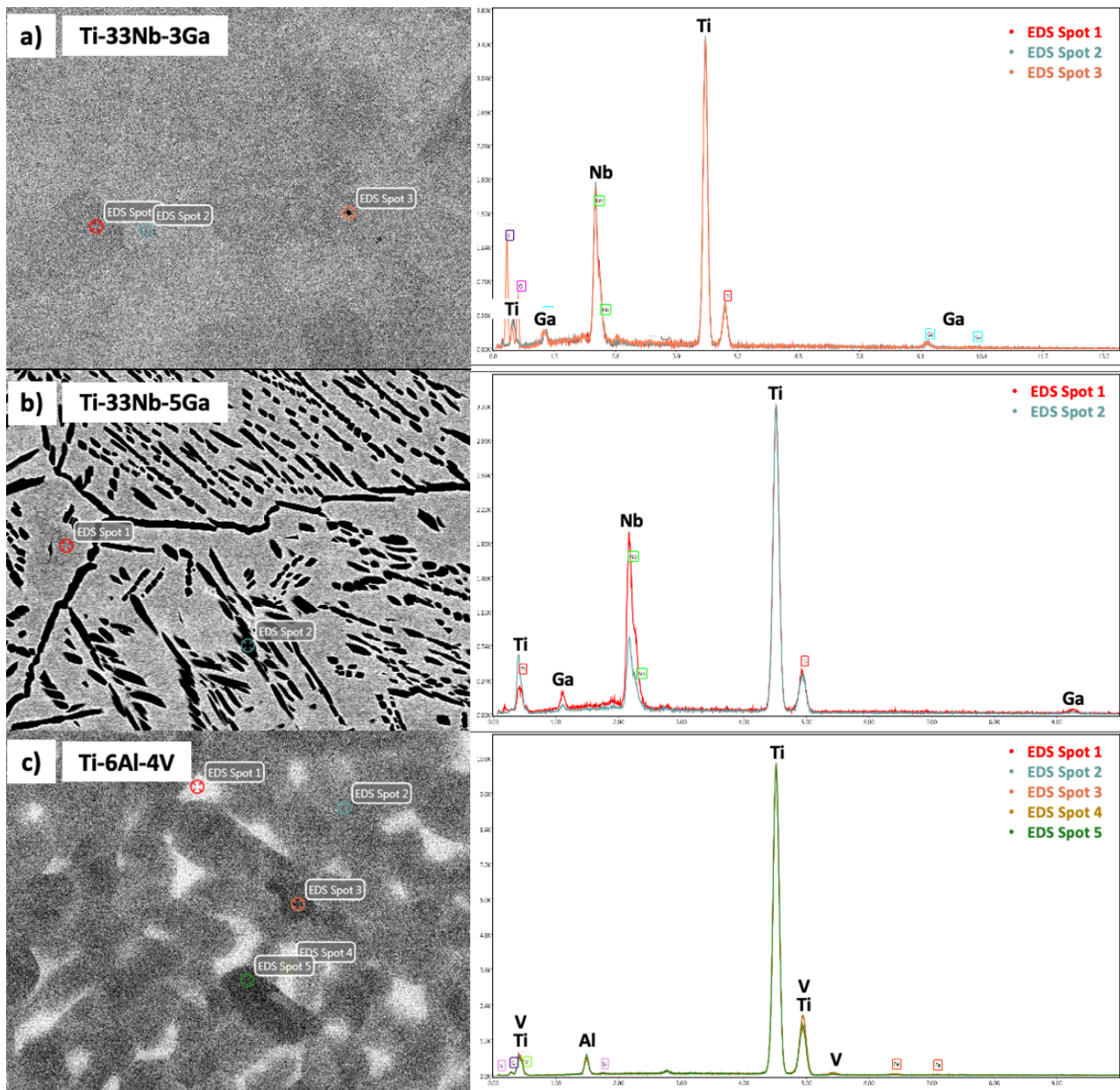


Figure 15: EDS spectrum analysis of polished samples indicating chemical composition of microstructural features and the overall alloy for a) Ti-33Nb-3Ga, b) Ti-33Nb-5Ga, and c) Ti-6Al-4V.

Electron backscatter diffraction (EBSD) and inverse pole figure (IPF) mapping of the β -phase grain structure, as exhibited for both alloys, reveals the various orientations of the β phase crystal lattice, as shown in Figure 16. Congregations of colour are indicative of the same lattice planes in crystal lattices, where the Miller indices of the pink, purple, orange, and blue assemblies correspond to 011, 101, $\bar{1}10$, and $\bar{1}02$ planes in the cubic crystal respectively. This indicates that the β -phase grains do not differ elementally, also confirmed by EDS in Figure 15a, and instead vary by the differing orientations of their crystal structure.

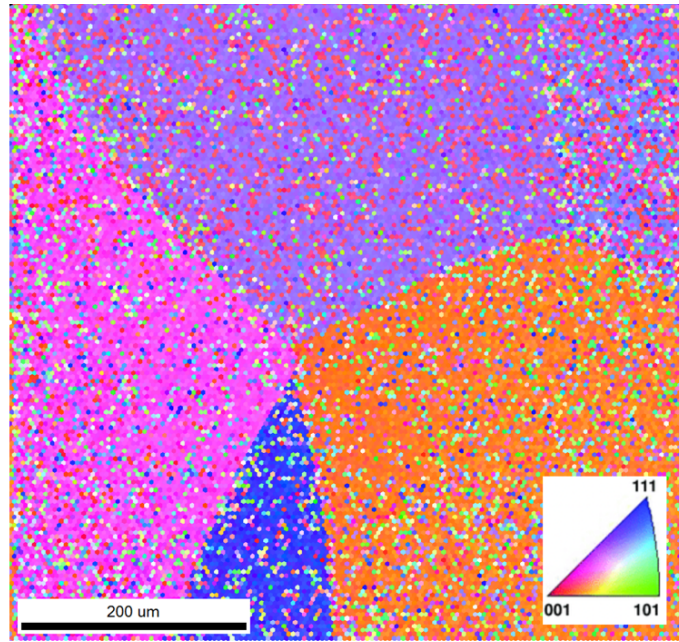


Figure 16: Inverse pole figure (IPF) map of the grains in polished Ti-33Nb-3Ga. Colours correspond to the Miller indices and therefore crystal structure orientations.

4.2 Mechanical Characterisation

4.2.1 Microhardness

The variation in Vickers microhardness as a function of increasing gallium content (wt%) compared to the reference material is depicted in Table 4 and Figure 17. Each of the developed alloys show microhardness values exceeding that of 200 HV, with values reported for Ti-33Nb-3Ga, Ti-33Nb-5Ga, and Ti-6Al-4V being 218.0 ± 2.9 , 260.9 ± 9.2 , and 297.0 ± 1.9 HV respectively (Table 4). Increasing elemental concentrations of gallium from 3 to 5 wt% resulted in a 17.9% difference in microhardness, indicating a clear strengthening effect from gallium addition. The microhardness result for Ti-6Al-4V is in accordance with values reported in the literature [70] [71], with a percent error of approximately 17.8%. Compared to the microhardness result for Ti-6Al-4V, the 3 wt% Ga alloy deviates in microhardness by 26.6%, while the 5 wt% Ga alloy presents a modest divergence of merely 12.2%.

Table 4: The mean microhardness values for each alloy in addition to the reference alloy. Standard deviation is given for each value based on 7 measurements.

Alloy	Mean Microhardness (HV)
Ti-33Nb-3Ga	218.0 ± 2.9
Ti-33Nb-5Ga	260.9 ± 9.2
Ti-6Al-4V	297.0 ± 1.9

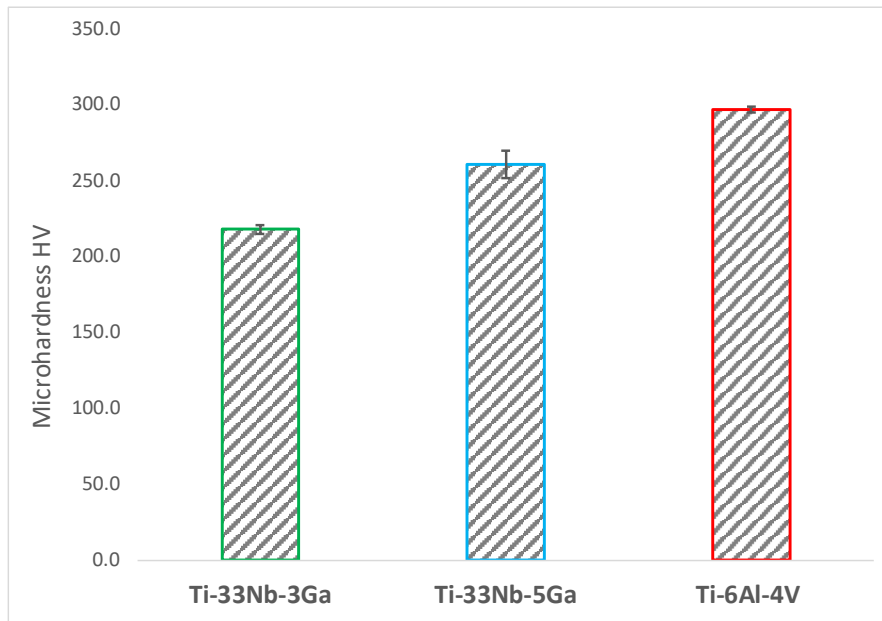


Figure 17: The mean Vickers microhardness (HV) for the developed alloys and the reference material based on 7 measurements. Errors bars informing standard deviation are provided.

4.2.2 Nanoindentation

The typical load versus displacement curves as obtained from nanoindentation tests are illustrated in Figure 18 for the Ti-33Nb-3Ga, Ti-33Nb-5Ga, and Ti-6Al-4V alloys under a maximum load of 100 mN. The load-depth curves reveal the loading, holding, and unloading stages, where the elastic recovery process is observed in the latter. The Oliver and Pharr (O-P) technique is used to calculate the Young's modulus and nanohardness, as per Equation 1, 2, 3.

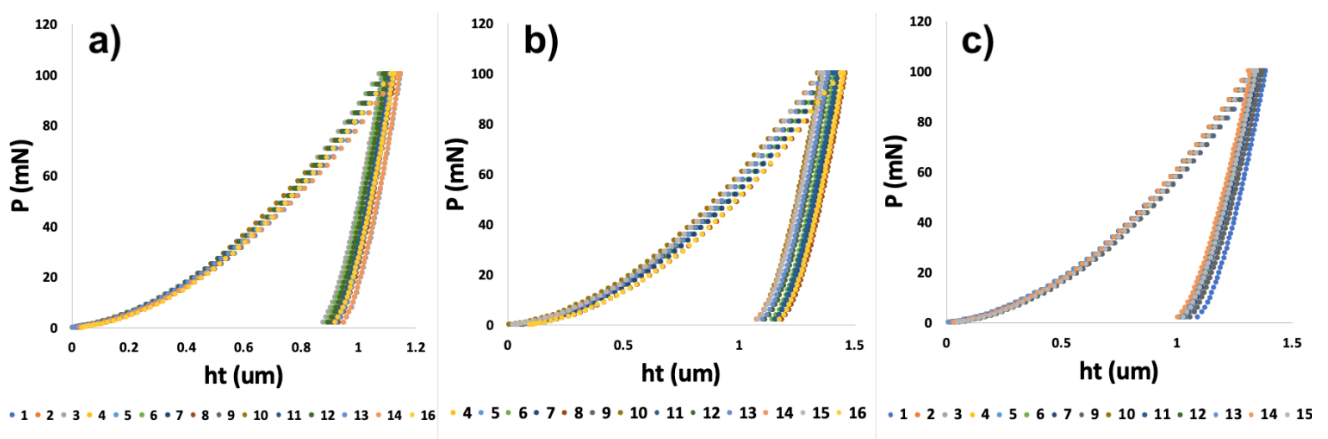


Figure 18: Load-displacement curves from nanoindentation results for a) Ti-33Nb-3Ga, b) Ti-33Nb-5Ga, and c) Ti-6Al-4V.

A comparison of the effect of increasing gallium content on the Young's modulus is depicted in Figure 19, where the mean results and standard deviation are reported in Table 5. The Young's modulus of Ti-33Nb-3Ga and Ti-33Nb-5Ga are evaluated to be 75.4 ± 2.4 GPa and 67.2 ± 1.6 GPa respectively. The measured Young's modulus result for the reference Ti-6Al-4V is 120.5 ± 2.3 GPa, which is in close agreement with reported literature values [72] [73] with a percent error of 9.5%. The addition of higher gallium concentrations from 3 to 5 wt% to the Ti-33Nb matrix led to a favourable decrease in the Young's modulus by 8.2 GPa, or a difference of 11.5%. Notably, both of the developed alloys have a reduced Young's modulus compared to the reference alloy, where the Young's modulus for the 3 wt% Ga sample was 37.4% less than Ti-6Al-4V, and the 5 wt% Ga alloy was lowered as much as 44.2% compared to the reference material.

Table 5: Mean \pm standard deviation of the Young's modulus and nanohardness results for the developed alloys together with the reference material as collected by nanoindentation (4x4 matrix).

Alloy	Mean Young's Modulus (GPa)	Mean Nanohardness (HV)
Ti-33Nb-3Ga	75.4 ± 2.4	239.5 ± 13.6
Ti-33Nb-5Ga	67.2 ± 1.6	274.3 ± 9.9
Ti-6Al-4V	120.5 ± 2.3	371.4 ± 13.0

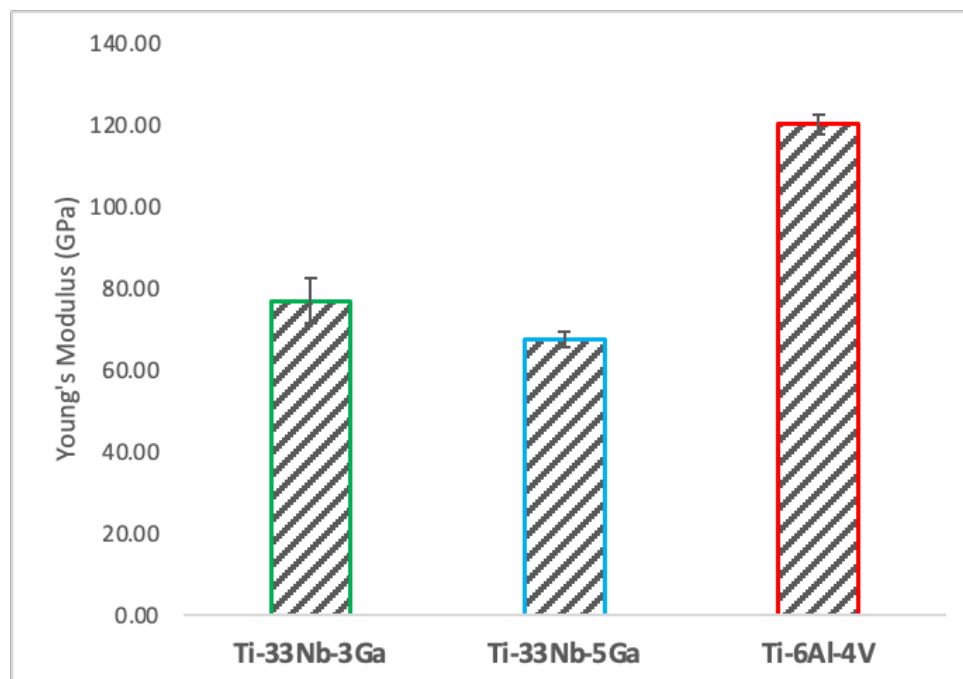


Figure 19: Young's modulus of the developed alloys and reference material collected by nanoindentation testing over a 4x4 matrix. Errors bars informing standard deviation are provided.

The effect of gallium addition on the nanohardness for the respective samples is depicted in Figure 20. Nanohardness values exhibit a strengthening effect with increasing gallium content, where the measured values for Ti-33Nb-3Ga and Ti-33Nb-5Ga were 239.5 ± 13.6 HV and 274.3 ± 9.9 HV respectively (Table 5). This result represents an increase in hardness of 13.6% between alloys. Comparatively, the reference alloy exhibited a nanohardness of 371.4 ± 13.0 HV which is similarly reported throughout literature [74], with a percent error of 6.41%.

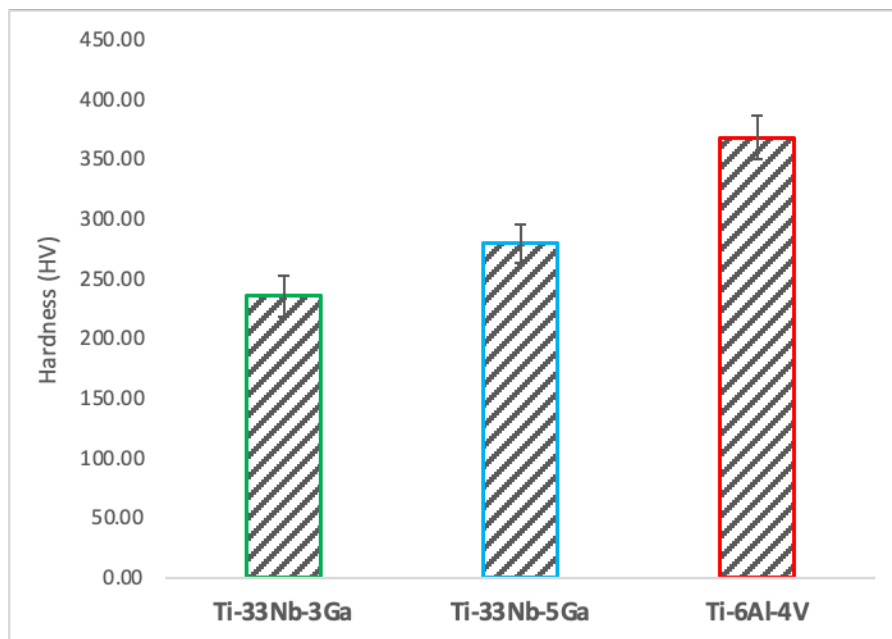


Figure 20: Nanohardness of the developed alloys and reference material collected by nanoindentation testing over a 4x4 matrix. Errors bars informing standard deviation are provided.

4.3 Biological Characterisation

4.3.1 Antimicrobial Activity Assay

The in-vitro antibacterial activity of Ti-33Nb-3Ga and Ti-33Nb-5Ga specimens, together with the reference Ti-6Al-4V, against Gram-negative *P. aeruginosa* and Gram-positive *S. aureus* bacteria is reported in Figure 21. The antibacterial rate was quantified over 6 and 24 hours, where both *P. aeruginosa* and *S. aureus* bacteria exhibited significant inhibition when directly seeded to the gallium-based alloys. For Ti-33Nb-3Ga and Ti-33Nb-5Ga, the antimicrobial rate observed against *P. aeruginosa* over 6 hours was $90 \pm 5\%$ and $95 \pm 3\%$ respectively (Figure 21A), while Ti-6Al-4V demonstrated a rate of $3 \pm 2\%$. Consequently, the inhibition of *S. aureus* bacteria over a 6 hour period was measured at $36.7 \pm 7.6\%$ and $50 \pm 5\%$ for 3 wt% and 5 wt% gallium samples respectively. Here, the bacterial inhibition exhibited by Ti-6Al-4V was merely $2 \pm 1\%$. Furthermore, after 24 hours, the antibacterial rate over *P.*

aeruginosa bacteria was measured at $30 \pm 1\%$ for Ti-33Nb-3Ga, $92.3 \pm 2.5\%$ for Ti-33Nb-5Ga, and $6.3 \pm 1.5\%$ for Ti-6Al-4V, as shown in Figure 21B. For *S. aureus*, the bactericidal effect over a 24 hour incubation indicates $30 \pm 10\%$ and $50 \pm 10\%$ inhibition by 3 and 5 wt% Ga-alloys respectively, while Ti-6Al-4V exhibited a rate of $4.7 \pm 1.5\%$.

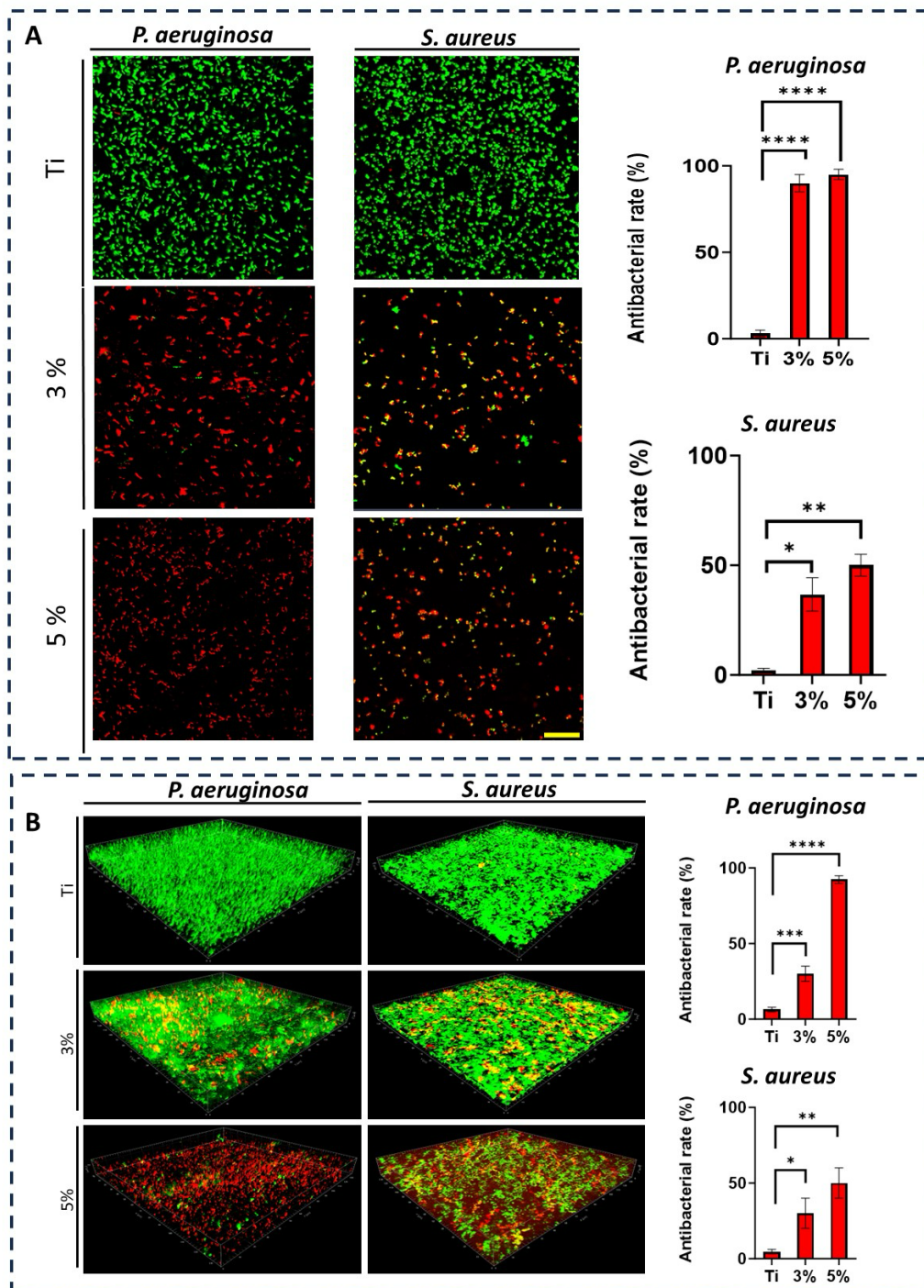


Figure 21: Ti-6Al-4V (labelled Ti), Ti-33Nb-3Ga (labelled 3%) and Ti-33Nb-5Ga (labelled 5%) antibacterial activities against Gram-negative *Pseudomonas aeruginosa* (*P. aeruginosa*) and Gram-positive *Staphylococcus aureus* (*S. aureus*). CLSM pictures and associated plots assessing the antibacterial efficiency of Ti, 3%, and 5% against *P. aeruginosa* and *S. aureus* for 6 hours (A) and 24 hours (B). Dead bacteria are red, while living bacteria are green. The scale bar measures 20 μm . $n = 3 \pm \text{SD}$. * $p < 0.1$, ** $p < 0.01$, *** $p < 0.001$, **** $p < 0.0001$.

The CLSM images of bacterial strains on the surfaces of the alloys were captured to further elucidate the antibacterial efficacies of the samples. Dead (red) and live (green) bacteria were observed using fluorescence staining. Figure 21A depicts the bacterial viability over 6 hour incubation, while Figure 21B shows the Z-stack surface rendered 3D models depicting the bacterial biovolume density for *P. aeruginosa* and *S. aureus* at 24 hours. Viability staining reveals a significantly high proportion of dead and metabolically inactive cells for both Ti-33Nb-3Ga and Ti-33Nb-5Ga alloys, where the 5 wt% sample exhibits abundant cell death. Notably, the reference Ti-6Al-4V alloy is predominated by live cells, indicating bacterial cell strains remained healthy. The results indicate that the Ti-33Nb-5Ga alloy achieved the highest percentage of nonviable cells in both Gram-negative and Gram-positive bacterial cells.

4.3.2 Cytotoxicity Assay

The cell viability of the hGF cells cultivated onto the surfaces of the Ti-33Nb-3Ga and Ti-33Nb-5Ga alloys, together with the control Ti-6Al-4V, are depicted in Figure 22 and in Table 6. The cell viability for the control group (Ti-6Al-4V) was normalised and compared to that of the 3 wt% and 5 wt% Ga samples, reported at $103.1 \pm 4.6\%$ and $94.9 \pm 8.2\%$ respectively. Among the tested alloys, there is no significant difference when comparing the cell viability obtained by the Ti-33Nb-3Ga and Ti-33Nb-5Ga alloy specimens to the control surface (Ti-6Al-4V) ($p < 0.05$). Therefore, high cell proliferation and no cytotoxicity was observed on hGF cells in direct contact with the specimens over 24 hours.

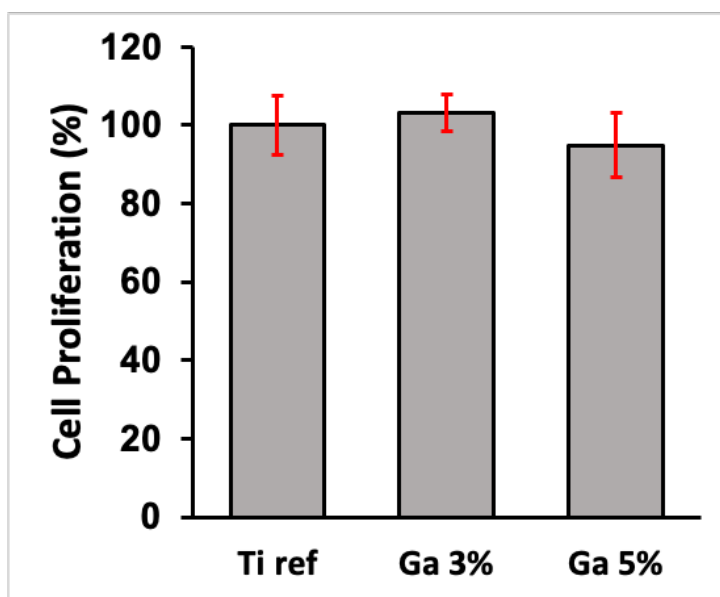


Figure 22: Cytocompatibility analysis of the alloys; values are representative of means and standard deviations. The assay showed that no toxic elements were released from the surface of the specimens as there was no significant difference ($p < 0.05$) between the designed alloys and the control after 24 hrs.

Table 6: Cytotoxicity assay results, described as means and standard deviations. The p-value is reported, where no significant difference ($p > 0.05$) is observed between alloys.

	Ti-6Al-4V Ref (normalised)	Ti-33Nb-3Ga	Ti-33Nb-5Ga
Mean Cell Proliferation	100	103.1	94.9
STDEV	7.6	4.6	8.2
P-value	-	0.414	0.29

Fluorescence images of the cell morphology and cytoskeleton distribution on the surface of the titanium samples are depicted in Figure 23. Images depict staining of actin cytoskeleton and nucleus with FITC conjugated phalloidin (green) and DAPI (blue) respectively. Cells directly exposed to alloys depict a healthy, typical morphology with a prominent nucleus, elongated fibroblastic spindle-shaped morphology, and F-actin filamentous stress fibres in a well-organised and defined structure of parallel bundles along the cellular axis. No significant difference is observable between Ti-33Nb-xGa specimens to the cytoskeleton distribution and cell morphology on the surface of the Ti-6Al-4V control. In addition, the cytoskeleton organisation is not affected by increasing elemental additions of gallium to the master alloy, evidenced by an absence of changed cell morphology and the lack of filament condensing. These results corroborate with the assay results in Figure 22 and Table 6. Images of stained cells in Figure 23 therefore clearly suggest the presence of healthy cells for the F-actin cytoskeleton and nucleus, indicating that the surfaces of the alloys are not cytotoxic.

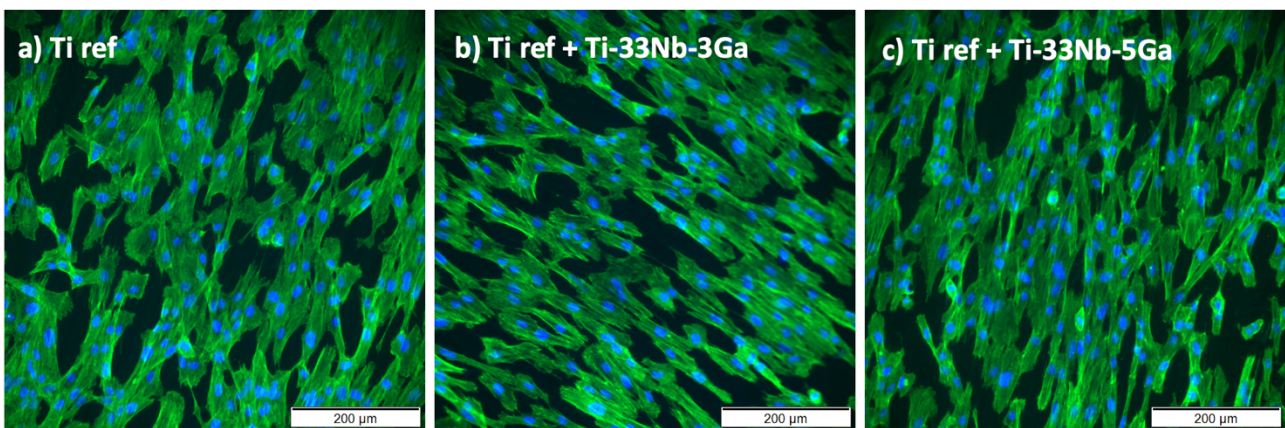


Figure 23: Cytoskeleton organisation and cell morphology imaged with an inverted microscope at 200 μm . Images depict stained F-actin (green) and nucleus (blue) for a) Ti-6Al-4V control, b) Ti-33Nb-3Ga, and c) Ti-33Nb-5Ga alloys.

5.0 DISCUSSION

5.1 Microstructural and Mechanical Evaluation

To address the literature gap that exists for new-generation β -phase Ti-Nb alloys and their inability to prevent biofilm formation while also maintaining low stiffness values, minor additions of gallium to Ti-33Nb alloys were investigated. Microstructural evaluation was conducted to reveal the expected mechanical performance and suitability of the alloys as biomaterials. The microstructure of the Ti-33Nb-3Ga alloy depicted equiaxed β -phase grains, with full retainment of a single bcc β -phase despite the addition of gallium. Retainment of a single β -phase is expected, as beta stabilisation is obtained from alloying with Nb, in addition to slow cooling rates maintained during casting. Consequently, the 5 wt% Ga alloy depicted slight retainment of bcc β -phase in the form of equiaxed grains shown in Figure 12e-f, however, the microstructure of this alloy was dominated by dendritic and interdendritic regions of α -phase colonies precipitated in the β -phase matrix. As this alloy contains greater concentrations of elemental gallium, this is an anticipated result due to the α -phase stabilisation provided by Ga. The size of dendrites directly correlates to the cooling rate of the alloy, where sufficiently fast cooling rates lead to martensitic transformation as shown in Figure 12c-d. As observed for Ti-33Nb-3Ga and parts of Ti-33Nb-5Ga, a retained single β -phase was detected, and is in agreement with Alberta et al. [9] for all alloys of Ti-45Nb-xGa ($x = 2, 4, 6, 8$ wt%). Though there is no evidence of alpha phases or martensitic transformation in their work, other new generation Ti-Nb alloys have shown dendritic features and α -phase transformation [75] [76] [77]. The microstructure of the reference alloy (Ti-6Al-4V), illustrated in Figure 13a-d, is also observed throughout literature, evidencing the α - β character [78] [79].

The intricate correlation between microstructure and mechanical properties aids in informing the underlying mechanisms that govern the material properties of the developed alloys. Optimised Young's modulus values are known to be obtained by retaining a β -phase microstructure, where gallium is an α stabiliser that may disrupt the beta phase stability by influencing titanium phase transformation ($T_{i_{\alpha \rightarrow \beta}} = 882$ °C, Figure 24). In contrast to this notion, the 5 wt% Ga alloy with multiple phases depicted the best reduction in Young's modulus, with a stiffness of 67.2 ± 1.6 GPa. This indicates that titanium alloys with multiple phases can decrease the Young's modulus, as also reported by [80]. The occurrence of martensitic transformation into the α' -phase has previously been recognized for its

contribution to reducing the Young's modulus, and when coupled with the presence of equiaxed grains in the β -phase, is believed to underpin this observed outcome [81] [28]. Furthermore, the replacement of titanium and niobium elements by smaller gallium atoms brings atoms closer together in the beta crystal lattice, potentially instigating further changes to the Young's modulus. Moreover, the improvements to the Young's modulus from Ti-33Nb-3Ga and Ti-33Nb-5Ga by 37.4% and 44.2% over the reference material is expected to significantly alleviate stress-shielding effects and bone resorption, resulting in minimised revision surgeries and diminished implant failure compared to Ti-6Al-4V. The microstructure of the bimodal Ti-6Al-4V alloy is abundant in primary α -phase grains with some retained transformed beta phases, which contributes to its high Young's modulus (Figure 13). Compared to earlier investigations on β -type Ti-Nb alloys, including [9, 65, 66, 82-85], the current outcomes improve on stiffnesses results previously reported. Alberta et al. [9] tested a series of Ti-45Nb-xGa ($x = 2, 4, 6, 8$ wt%) alloys and observed Young's modulus values within the range of 73.0 to 82.5 GPa. Notably, Young's moduli from [9] exceed those obtained within the present study by 6.1 to 9.1%, underlining the novelty of the present results and their contribution to bridging gaps within the literature.

Figure has been removed in open access version due to Copywrite restrictions.

Figure 24: Phase diagram for titanium-niobium alloys [86].

The presence of light and dark β -phase grains does not correlate with elemental differences, as previously noted in the case of α -phase dendrites (richer in Ti) surrounded in β -phase matrix (richer in Nb and Ga) for Ti-33Nb-5Ga (Figure 14, Figure 15). The IPF map depicted in Figure 16 indicates that variations in grains correspond to differences in the crystal structure orientation. Notably, the bonding force between atoms is restricted to the crystal structure, in addition to the distance between atoms, and is known to affect the Young's modulus. As the distance between atoms in Ti-33Nb-3Ga and Ti-33Nb-5Ga alloys have not been affected by heat treatment processes or plastic deformation, the Young's modulus values are believed to have been influenced by the crystal lattice orientations within the alloys. These orientations, and therefore their effect on the Young's modulus, are postulated to have been induced by Ga alloying additions on the distances between atoms.

Grain refinement is observed for the β -phase character of the Ti-33Nb-3Ga and Ti-33Nb-5Ga microstructures, where grain refinement has previously been reported in literature to influence the hardness properties of alloys. Shown in Figure 11 and Figure 12e-f, both alloys possess equiaxed β -grains, where the 5 wt% Ga alloy contains finer average grain sizes.

The microhardness results for Ti-33Nb-3Ga and Ti-33Nb-5Ga from both Vickers microhardness (218 ± 2.9 HV and 260.9 ± 9.2 HV respectively) and nanoindentation (239.5 ± 13.6 HV and 274.3 ± 9.9 HV respectively) methods are in agreement that Ti-33Nb-3Ga possesses a lower hardness than that of the Ti-33Nb-5Ga alloy. Hardness results therefore reveal a strengthening effect of gallium addition to the Ti-33Nb master alloy. This behaviour can be correlated to the reduced size of the β -phase equiaxed grains in this alloy, where it is believed that the presence of Ga atoms reduces the surface energy mismatch among crystal structure surfaces. This pinning effect halts the growth of grains, lessening their size and subsequently increasing the homogeneity of the microstructure. Furthermore, the presence of precipitated dendritic α -phases in Ti-33Nb-5Ga (Figure 12a-c), in addition to martensitic transformation, also contributes to an increase in hardness compared to the single β -phase exhibited in the 3 wt% Ga alloy. An augmented concentration of gallium is believed to have led to a higher occurrence of alpha precipitations, subsequently leading to an increase in hardness. It is probable that the α -phase played a vital role in strengthening the 5 wt% Ga alloy by impeding dislocations. Such hardness findings serve as vital indicators of the aptness of these alloys for biomedical implant applications. When combined with the Young's modulus results, both alloys show promising mechanical properties, with particular emphasis on the 5 wt% variant, showcasing mechanical properties that either surpass or, in the case of hardness, are just short of being at parity with the currently employed clinical Ti-6Al-4V alloy. However, analysis of the wear properties is necessitated to evaluate if the hardness is sufficiently high to prevent the incidence of wear. This would further inform the life span of the alloys when implanted, and their subsequent suitability.

The microhardness and nanohardness values of the novel alloys closely approach the hardness level of the reference alloy, exhibiting a notable consistency with results documented in the literature for Ti-Nb alloys characterized by a predominant β -phase matrix [9, 66]. Furthermore, results show improved hardness values over numerous previously reported Ti-Nb alloys, including [2, 22, 87, 88]. However, as illustrated in Figure 25, a significant divergence between the microhardness and nanohardness results becomes apparent. Deviation of nanohardness in the range of 10-30% magnitudes larger than the microhardness is well reported in literature and is owed to measuring the projected contact area at the peak load during nanoindentation, compared to measuring the residual projected area in microhardness measurements. Because the residual projected area is always greater than that of the projected contact area at peak load, microhardness values are consistently lower than the nanohardness. Regardless of this facet, a clear strengthening

effect is exhibited from both methods when alloying additions of gallium to the matrix of the Ti-33Nb master alloy is increased.

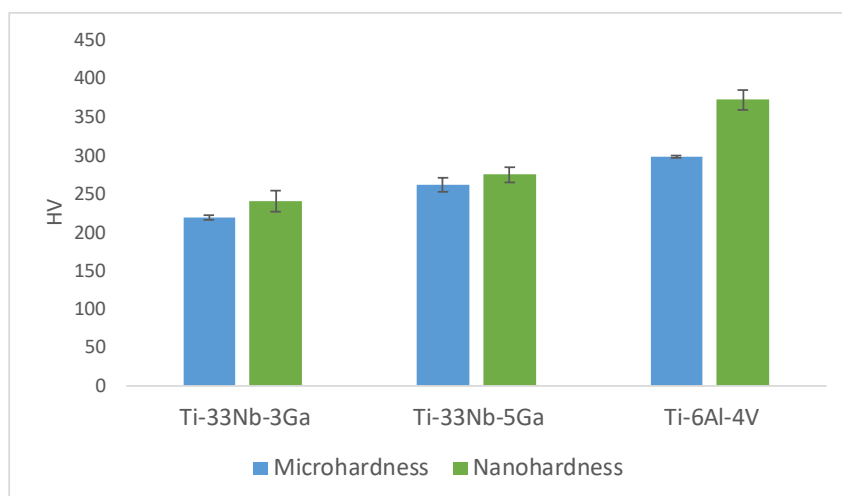


Figure 25: Comparison of results collected from microhardness and nanohardness methods for all alloys.

5.2 Biological Evaluation

The emergence of new generation β -phase Ti-Nb alloys that show excellent mechanical properties and biocompatibility are limited by their inability to prevent biofilm formation, which may ultimately result in implant failure. Biofilms are formed by bacteria colonising into diverse populations in the autogenous extracellular matrix on the surfaces of medical implant devices, where both Gram-negative and Gram-positive bacteria lead to such infections. The significant antibacterial properties of both Ti-33Nb-3Ga and Ti-33Nb-5Ga alloys against Gram-negative (*P. aeruginosa*) and Gram-positive (*S. aureus*) bacteria is revealed in Figure 21. Both alloys depict significant antimicrobial action, with the best results being against *P. aeruginosa* cells over 6 hours. Antibacterial activity up to $90 \pm 5\%$ for the 3 wt% alloy was observed, in addition to $95 \pm 3\%$ for the 5 wt% alloy. At 24 hour incubation, the potency of Ti-33Nb-3Ga against *P. aeruginosa* decreased to $30 \pm 5\%$, while the Ti-33Nb-5Ga alloy remained unchanged at $92.3 \pm 2.5\%$. This indicates that the 5 wt% Ga alloy exhibits significantly elevated and prolonged antimicrobial potency against Gram-negative bacteria, regardless of time. This includes as much as a 101.9% increase in antimicrobial properties over that of Ti-33Nb-3Ga. Furthermore, inhibition results against *S. aureus* depict the same trends, confirming that increased alloying additions of gallium are advantageous to the antimicrobial properties. Notably, the smaller antimicrobial impact observed for all alloys in *S. aureus* bacteria may be attributed to the more complex cell wall in Gram-negative bacteria [44]. This may slow gallium ion penetration and limit efflux mechanisms, ultimately leading

to a smaller concentration of gallium in the intracellular region, and therefore smaller inhibitions.

Both Ga-based alloys exhibit significant improvement in the antibacterial potency when compared to the presently employed Ti-6Al-4V implant material. This includes surpassing the antimicrobial rate of Ti-6Al-4V by a substantial margin, within the range of 130.3% to 187.8%. The mechanism for the observed antibacterial effect within the Ga-based alloys is theorised to employ a “Trojan horse” strategy of bacterial inhibition, which has been studied extensively [13, 89-91]. Gallium ions (Ga^{3+}) possess an analogous ionic radius, electron affinity, and ionisation potential to that of ferric ions (Fe^{3+}) and may therefore be mistaken for Fe^{3+} and bind strongly with iron-binding proteins involved in the metabolic and signalling processes of bacteria [17, 50, 53]. Siderophores are produced by bacterial cells and possess iron uptake systems, where Ga^{3+} competes with Fe^{3+} for binding to siderophores and essential enzymes and proteins [13]. Gallium is not redox-active, and when bound with iron-binding proteins can inhibit various iron-dependent redox pathways, and ultimately the function and subsistence of the bacterial cell [13, 89, 91]. By comparing their antibacterial efficacy, it becomes evident that Ti-33Nb-3Ga and Ti-33Nb-5Ga possess a superior capacity to inhibit biofilm formation, consequently reducing the likelihood of implant failure and the need for revision surgeries in comparison to the currently utilized Ti-6Al-4V.

Although there is a lack of literature existing for gallium-based materials, with a particular gap relating to gallium-based alloy systems, the antibacterial properties of Ti-33Nb-3Ga and Ti-33Nb-5Ga represent improved values compared to those reported previously for gallium material systems in literature, including [14, 15, 34, 44, 49, 56, 61]. Notably, most of the literature examines materials with gallium coatings and are therefore expected to be more potent over shorter times compared to metallurgically added Ga. However, the results in this study show stronger inhibition of bacteria over previous gallium-coated systems. For example, commercial titanium alloys coated with GaCis and GaOss ($\text{Ga}(\text{NO}_3)_3$) depicted a 27-35% decrease in *A. baumannii* [14, 61]. The results in this thesis show an improvement in this value by as much as 111.5%. This is particularly notable, as alloys with metallurgical additions of gallium are more likely to retain their antimicrobial efficacies, while gallium-coated biomaterials are generally more susceptible to wear in the body, consequently diminishing their potency over time. Furthermore, to the author’s knowledge, Cochis et al. [15] is the only study to have examined the antibacterial activity of titanium alloys with elemental gallium additions. In this work, 1, 2 and 24 wt% Ga additions to Ti-Al-Zr-Si observed a reduction in viability at a maximum of 80-95%. However, the master alloy would

likely exhibit high stiffness values due to the absence of niobium, where the alloy also contains toxic alloying additions of Al. The developed Ti-33Nb-5Ga alloy therefore demonstrates antimicrobial results that are not only comparable but superior to that reported in [15].

The investigation of in-vitro biocompatibility and cell proliferation yielded favourable results, indicating the absence of cytotoxicity in all alloys. The in-vitro viability of the hGF cell line in direct contact with alloy surfaces over 24 hours was evaluated. Results in Figure 22 reveal that both Ti-33Nb-3Ga and Ti-33Nb-5Ga support cell viability that does not significantly differ from the control Ti-6Al-4V ($p < 0.05$), with mean cell proliferations of $103.1 \pm 4.6\%$ and $94.9 \pm 8.9\%$ respectively. These conclusions are afforded as the statistical analysis of the p-value for both alloys is less than 0.05. Furthermore, cell morphology and cytoskeleton distribution on the surfaces of the alloys was imaged after F-actin staining procedures, as shown in Figure 23. The F-actin cytoskeleton is a critical cell structure to cellular functions such as division, intracellular transport, signalling pathways, and gene expression, as well as in mechano-transduction and motility mechanisms associated with differentiation [92]. Due to the stability afforded by F-actin and its active collaboration with cellular function, as well as its responsiveness to surrounding environment, the F-actin cytoskeleton is a preliminary indicator of cytotoxicity [92]. Because no deleterious effects to the structure were evidenced in cell staining, such as changes to cell morphology and condensing, alloys depict obvious biocompatibilities with no cytotoxicity. Both alloys show images consistent with healthy cell morphology and cytoskeleton, such as a prominent nucleus and elongated fibroblastic spindle-shaped morphology. These results inform the biocompatibility of the alloys for potential implantation in orthopaedic biomedical applications and are in accordance with previous studies. Gallium has previously been reported to be a safe metal for use in biomedical applications by [93-96]. For example, metallurgical addition of gallium in 1-2 wt% up to 23 wt% observed no cytotoxicity in human fetal progenitor and human osteosarcoma cell lines [15].

5.3 Limitations of this Study

The inherent limitations exhibited throughout this study, as manifested in the results, provide valuable insights for their prospective resolution in future research endeavours. Due to the investigation of merely two novel alloys, trends correlated to increasing Ga content could not be entirely elucidated. Further exploration of various gallium compositions added to Ti-33Nb is therefore warranted, for example in 1, 7, and 9 wt% additions, with a focus on

comparing the outcomes to the master alloy devoid of any gallium. In addition, size restraints of the casted alloys prevented tensile testing to evaluate a greater range of mechanical properties, such as tensile yield strength, ultimate tensile strength, tensile strain, and elastic energy. These properties would better inform the suitability of the alloys as biomaterials, where collection of such data would benefit future studies. Furthermore, although the mechanical properties of both alloys were exceptionally encouraging, the effect of subjecting alloys to different processing parameters could show further improvements in mechanical properties. It is widely recognised that a reduction in Young's modulus can be observed by controlling thermomechanical treatments; and therefore, the phase transformations. This could potentially result in further optimisation of the mechanical properties reported in this study. Finally, biocompatibility was assessed over 24 hours and revealed that no cytotoxicity was exhibited for either alloy. However, further validation of this outcome could be investigated by measuring the effect of the alloys over a sustained time frame, and within different cell lines – for example, in human fetal progenitor and human osteosarcoma cell lines.

6.0 CONCLUSIONS & SUGGESTIONS FOR FUTURE WORK

6.1 Conclusions

Two novel alloys with minor gallium addition (Ti-33Nb-3Ga, Ti-33Nb-5Ga) were developed and assessed in terms of their microstructural, mechanical, antibacterial, and cytotoxic properties. The microstructures display homogenous equiaxed β -phase grains, whereby increasing Ga content to 5 wt% led to precipitation of dendritic α -phase colonies rich in titanium surrounded by a β -phase matrix enriched with niobium and gallium. Martensitic transformation to α'' was also observed in Ti-33Nb-5Ga. The homogenous, equiaxed bcc β -phase grains show differences in their crystal structure orientation, evidenced by IPF mapping. Furthermore, grain refinement was observed from increasing

Ga content and is believed to have influenced the hardness of alloys. The addition of Ga resulted in Young's modulus values (75.4 and 67.2 GPa) significantly lower than that of medical grade Ti-6Al-4V (120.5 GPa), as much as 44.2%. These results inform the suitability of both alloys, notably the 5 wt% Ga alloy, as implant biomaterials by possessing stiffness values closer to cortical bone, where stress shielding effects and therefore implant failure would be minimised. Moreover, the microhardness (218.0 and 260.9 HV) and nanohardness (239.5 and 274.3 HV) results reveal the strengthening effect of gallium addition to the Ti-33Nb master alloy, with results slightly lower than that of commercial Ti-6Al-4V. Therefore, the addition of gallium yields high hardness values paired with significantly reduced Young's moduli. Furthermore, the presence of gallium even in small amounts (3, 5 wt%) to the titanium master alloy depicted highly efficient antibacterial function, with the best results being against *P. aeruginosa* cells over 6 hours. Antibacterial activity up to $90 \pm 5\%$ for the 3 wt% alloy was observed, in addition to $95 \pm 3\%$ for the 5 wt% alloy. These results indicate an improvement over the antimicrobial rate of Ti-6Al-4V by as much as 130.3% and 187.8%. However, after 24 hours, the potency of Ti-33Nb-3Ga decreased, while the Ti-33Nb-5Ga alloy remained unchanged at $92.3 \pm 2.5\%$. These results suggest that the 5 wt% Ga alloy exhibits the highest and most prolonged antimicrobial potency. From CLSM images, both alloys not only inhibit bacterial growth but also induce cell death in both Gram-negative and Gram-positive bacteria. Furthermore, each of the alloys also depict no cytotoxicity in the presence of hGF cell lines. This suggests that biofilm formation, revision surgeries, and implant failure would likely be minimised compared to conventional clinical Ti-6Al-4V. These results, paired with the mechanical properties and the exclusion of any toxic elements, indicate the potential application of both alloys as promising biomedical materials that could improve patient outcomes.

6.2 Suggestions for Future Work

Although promising findings regarding the microstructure, mechanical properties, antimicrobial action, and cytotoxicity of the alloys has been reported, further research is warranted to explore their comprehensive properties. Suggestions for future work include investigating larger alloying additions of gallium (wt%) and their effect on the results. More extensive mechanical property evaluation could be attained by ultrasonic pulse-echo methods in addition to tensile and compressive loading studies. Such methods could aid in elucidating bulk modulus, Poisson's ratio, in addition to tensile and compressive yield strength, ultimate tensile strength, tensile strain, and elastic energy. These mechanical properties will better inform the suitability of alloys for implantation. Analysis of wear,

tribocorrosion and fatigue life would also be beneficial in investigating the characteristics of implant materials. Furthermore, study into corrosion resistance is suggested to be evaluated by linear anodic polarization and open circuit potential (OCP) monitoring. The release kinetics of the alloys should be studied in simulated bodily fluids to evaluate corrosion resistance, and whether increased Ga addition is deleterious. More extensive cytotoxicity and antimicrobial studies should also be conducted to understand the long-term effect of the alloys in-vitro over various time points. Study into more extensive direct and indirect osteointegration and osteogenic differentiation is also warranted to assess the suitability of alloys for use in in-vivo biomedical applications.

REFERENCES

- [1] S. Scialla, G. Martuscelli, F. Nappi, S.S.A. Singh, A. Iervolino, D. Larobina, L. Ambrosio, M.G. Raucci, Trends in Managing Cardiac and Orthopaedic Device-Associated Infections by Using Therapeutic Biomaterials, *Polymers (Basel)* 13(10) (2021).
- [2] Y.L. Hao, S.J. Li, S.Y. Sun, R. Yang, Effect of Zr and Sn on Young's modulus and superelasticity of Ti-Nb-based alloys, *Materials Science and Engineering a-Structural Materials Properties Microstructure and Processing* 441(1-2) (2006) 112-118.
- [3] E.L. Zhang, F.B. Li, H.Y. Wang, J. Liu, C.M. Wang, M.Q. Li, K. Yang, A new antibacterial titanium-copper sintered alloy: Preparation and antibacterial property, *Materials Science & Engineering C-Materials for Biological Applications* 33(7) (2013) 4280-4287.
- [4] M. Calin, A. Helth, J.J.G. Moreno, M. Bonisch, V. Brackmann, L. Giebeler, T. Gemming, C.E. Lekka, A. Gebert, R. Schnettler, J. Eckert, Elastic softening of beta-type Ti-Nb alloys by indium (In) additions, *Journal of the Mechanical Behavior of Biomedical Materials* 39 (2014) 162-174.
- [5] P. Afzali, R. Ghomashchi, R.H. Oskouei, On the Corrosion Behaviour of Low Modulus Titanium Alloys for Medical Implant Applications: A Review, *Metals* 9(8) (2019) 878.
- [6] K. Fallahnezhad, R.H. Oskouei, H. Badnava, M. Taylor, The Influence of Assembly Force on the Material Loss at the Metallic Head-Neck Junction of Hip Implants Subjected to Cyclic Fretting Wear, *Metals* 9(4) (2019) 422.

- [7] M. Feyzi, K. Fallahnezhad, M. Taylor, R. Hashemi, The mechanics of head-neck taper junctions: What do we know from finite element analysis?, *Journal of the Mechanical Behavior of Biomedical Materials* 116 (2021) 104338.
- [8] H. Farhoudi, K. Fallahnezhad, R.H. Oskouei, M. Taylor, A finite element study on the mechanical response of the head-neck interface of hip implants under realistic forces and moments of daily activities: Part 1, level walking, *Journal of the Mechanical Behavior of Biomedical Materials* 75 (2017) 470-476.
- [9] L.A. Alberta, Y. Fortouna, J. Vishnu, S. Pilz, A. Gebert, C. Lekka, K. Nielsch, M. Calin, Effects of Ga on the structural, mechanical and electronic properties of β -Ti-45Nb alloy by experiments and ab initio calculations, *J Mech Behav Biomed* 140 (2023).
- [10] J.S. Wang, W.L. Xiao, L. Ren, Y. Fu, C.L. Ma, The roles of oxygen content on microstructural transformation, mechanical properties and corrosion resistance of Ti-Nb-based biomedical alloys with different beta stabilities, *Materials Characterization* 176 (2021).
- [11] E. Inan-Eroglu, A. Ayaz, Is aluminum exposure a risk factor for neurological disorders?, *J Res Med Sci* 23 (2018) 51.
- [12] C.C. Gomes, L.M. Moreira, V.J. Santos, A.S. Ramos, J.P. Lyon, C.P. Soares, F.V. Santos, Assessment of the genetic risks of a metallic alloy used in medical implants, *Genet Mol Biol* 34(1) (2011) 116-21.
- [13] J.A. Lemire, J.J. Harrison, R.J. Turner, Antimicrobial activity of metals: mechanisms, molecular targets and applications, *Nat Rev Microbiol* 11(6) (2013) 371-84.
- [14] A. Cochis, B. Azzimonti, C. Della Valle, E. De Giglio, N. Bloise, L. Visai, S. Cometa, L. Rimondini, R. Chiesa, The effect of silver or gallium doped titanium against the multidrug resistant *Acinetobacter baumannii*, *Biomaterials* 80 (2016) 80-95.
- [15] A. Cochis, B. Azzimonti, R. Chiesa, L. Rimondini, M. Gasik, Metallurgical Gallium Additions to Titanium Alloys Demonstrate a Strong Time-Increasing Antibacterial Activity without any Cellular Toxicity, *ACS Biomater Sci Eng* 5(6) (2019) 2815-2820.
- [16] S. Ozan, J.X. Lin, Y.C. Li, R. Ipek, C. Wen, Development of Ti-Nb-Zr alloys with high elastic admissible strain for temporary orthopedic devices, *Acta Biomaterialia* 20 (2015) 176-187.
- [17] C.Q. Ning, D.Y. Ding, K.R. Dai, W.Y. Zhai, L. Chen, The effect of Zr content on the microstructure, mechanical properties and cell attachment of Ti-35Nb-xZr alloys, *Biomedical Materials* 5(4) (2010).
- [18] Y.L. Hao, S.J. Li, S.Y. Sun, C.Y. Zheng, R. Yang, Elastic deformation behaviour of Ti-24Nb-4Zr-7.9Sn for biomedical applications, *Acta Biomater* 3(2) (2007) 277-86.
- [19] Y.Y. Guo, D.S. Chen, W.J. Lu, Y.H. Jia, L.Q. Wang, X.L. Zhang, Corrosion resistance and in vitro response of a novel Ti35Nb2Ta3Zr alloy with a low Young's modulus, *Biomedical Materials* 8(5) (2013).
- [20] S. Bahl, S. Das, S. Suwas, K. Chatterjee, Engineering the next-generation tin containing beta titanium alloys with high strength and low modulus for orthopedic applications, *Journal of the Mechanical Behavior of Biomedical Materials* 78 (2018) 124-133.
- [21] R. Banerjee, S. Nag, S. Samuel, H.L. Fraser, Laser-deposited Ti-Nb-Zr-Ta orthopedic alloys, *J Biomed Mater Res A* 78(2) (2006) 298-305.
- [22] E. Bertrand, T. Gloriant, D.M. Gordin, E. Vasilescu, P. Drob, C. Vasilescu, S.I. Drob, Synthesis and characterisation of a new superelastic Ti-25Ta-25Nb biomedical alloy, *J Mech Behav Biomed Mater* 3(8) (2010) 559-64.
- [23] A. Biesiekierski, J. Wang, M.A.H. Gepreel, C. Wen, A new look at biomedical Ti-based shape memory alloys, *Acta Biomaterialia* 8(5) (2012) 1661-1669.
- [24] Y. Fu, J. Wang, W. Xiao, X. Zhao, C. Ma, Microstructure evolution and mechanical properties of Ti-8Nb-2Fe-0.2O alloy with high elastic admissible strain for orthopedic implant applications, *Progress in Natural Science: Materials International* 30(1) (2020) 100-105.
- [25] Y. Fu, W. Xiao, J. Wang, L. Ren, X. Zhao, C. Ma, A novel strategy for developing $\alpha + \beta$ dual-phase titanium alloys with low Young's modulus and high yield strength, *Journal of Materials Science & Technology* 76 (2021) 122-128.
- [26] J. Wang, W. Xiao, Y. Fu, L. Ren, B. Song, C. Liu, C. Ma, Effects of initial microstructure on the aging behavior and subsequent mechanical properties of Ti-Nb-O titanium alloy, *Journal of Materials Research* 37(14) (2022) 2304-2313.
- [27] S. Hanada, H. Matsumoto, S. Watanabe, Mechanical compatibility of titanium implants in hard tissues, *International Congress Series* 1284 (2005) 239-247.

- [28] M.H.C. Tan, A.D. Baghi, R. Ghomashchi, W. Xiao, R.H. Oskouei, Effect of niobium content on the microstructure and Young's modulus of Ti-xNb-7Zr alloys for medical implants, *J Mech Behav Biomed Mater* 99 (2019) 78-85.
- [29] C.Y. Mao, W.J. Yu, M. Jin, Y.C. Wang, X.Q. Shang, L. Lin, X.Q. Zeng, L.Q. Wang, E.Y. Lu, Mechanobiologically optimized Ti-35Nb-2Ta-3Zr improves load transduction and enhances bone remodeling in tilted dental implant therapy, *Bioactive Materials* 16 (2022) 15-26.
- [30] C.H. Park, C.S. Lee, Y.J. Kim, J.H. Jang, J.Y. Suh, J.W. Park, Improved pre-osteoblast response and mechanical compatibility of ultrafine-grained Ti-13Nb-13Zr alloy, *Clinical Oral Implants Research* 22(7) (2011) 735-742.
- [31] B. Bai, E.L. Zhang, H. Dong, J. Liu, Biocompatibility of antibacterial Ti-Cu sintered alloy: in vivo bone response, *Journal of Materials Science-Materials in Medicine* 26(12) (2015).
- [32] J. Fu, A. Yamamoto, H.Y. Kim, H. Hosoda, S. Miyazaki, Novel Ti-base superelastic alloys with large recovery strain and excellent biocompatibility, *Acta Biomaterialia* 17 (2015) 56-67.
- [33] F.P. Li, F.X. Liu, K. Huang, S.B. Yang, Advancement of Gallium and Gallium-Based Compounds as Antimicrobial Agents, *Frontiers in Bioengineering and Biotechnology* 10 (2022).
- [34] T.J. Keenan, L.M. Placek, M.M. Hall, A.W. Wren, Antibacterial and antifungal potential of Ga-bioactive glass and Ga-bioactive glass/polymeric hydrogel composites, *Journal of Biomedical Materials Research Part B-Applied Biomaterials* 105(5) (2017) 1102-1113.
- [35] G.E. Stan, T. Tite, A.C. Popa, I.M. Chirica, C.C. Negrila, C. Besleaga, I. Zgura, A.C. Sergentu, G. Popescu-Pelin, D. Cristea, L.E. Ionescu, M. Neculescu, H.R. Fernandes, J.M.F. Ferreira, The Beneficial Mechanical and Biological Outcomes of Thin Copper-Gallium Doped Silica-Rich Bio-Active Glass Implant-Type Coatings, *Coatings* 10(11) (2020).
- [36] A.R. Yazdi, L. Torkan, W. Stone, M.R. Towler, The impact of gallium content on degradation, bioactivity, and antibacterial potency of zinc borate bioactive glass, *Journal of Biomedical Materials Research Part B-Applied Biomaterials* 106(1) (2018) 367-376.
- [37] A.R. Yazdi, L. Torkan, S.D. Waldman, M.R. Towler, Development of a novel bioactive glass suitable for osteosarcoma-related bone grafts, *Journal of Biomedical Materials Research Part B-Applied Biomaterials* 106(3) (2018) 1186-1193.
- [38] N. Mutlu, F. Kurtuldu, I. Unalan, Z. Nešćáková, H. Kaňková, D. Galusková, M. Michálek, L. Liverani, D. Galusek, A.R. Boccaccini, Effect of Zn and Ga doping on bioactivity, degradation, and antibacterial properties of borate 1393-B3 bioactive glass, *Ceram Int* 48(11) (2022) 16404-16417.
- [39] S.P. Valappil, D. Ready, E.A. Abou Neel, D.M. Pickup, W. Chrzanowski, L.A. O'Dell, R.J. Newport, M.E. Smith, M. Wilson, J.C. Knowles, Antimicrobial gallium-doped phosphate-based glasses, *Advanced Functional Materials* 18(5) (2008) 732-741.
- [40] R. Sahdev, T.I. Ansari, S.M. Higham, S.P. Valappil, Potential use of gallium-doped phosphate-based glass material for periodontitis treatment, *Journal of Biomaterials Applications* 30(1) (2015) 85-92.
- [41] S.P. Valappil, M. Coombes, L. Wright, G.J. Owens, R.J.M. Lynch, C.K. Hope, S.M. Higham, Role of gallium and silver from phosphate-based glasses on in vitro dual species oral biofilm models of *Porphyromonas gingivalis* and *Streptococcus gordonii*, *Acta Biomaterialia* 8(5) (2012) 1957-1965.
- [42] S. Pourshahrestani, E. Zeimaran, N.A. Kadri, N. Gargiulo, S. Samuel, S.V. Naveen, T. Kamarul, M.R. Towler, Gallium-containing mesoporous bioactive glass with potent hemostatic activity and antibacterial efficacy, *Journal of Materials Chemistry B* 4(1) (2016) 71-86.
- [43] A.J. Salinas, M. Vallet-Regi, Glasses in bone regeneration: A multiscale issue, *Journal of Non-Crystalline Solids* 432 (2016) 9-14.
- [44] D.Q. Pham, S. Gangadoo, C.C. Berndt, J. Chapman, J. Zhai, K. Vasilev, V.K. Truong, A.S.M. Ang, Antibacterial Longevity of a Novel Gallium Liquid Metal/Hydroxyapatite Composite Coating Fabricated by Plasma Spray, *ACS Applied Materials & Interfaces* 14(16) (2022) 18974-18988.
- [45] L. Li, H. Chang, N. Yong, M.X. Li, Y. Hou, W. Rao, Superior antibacterial activity of gallium based liquid metals due to Ga³⁺ induced intracellular ROS generation, *Journal of Materials Chemistry B* 9(1) (2021).
- [46] S. Cheeseman, A. Elbourne, S. Gangadoo, Z.L. Shaw, S.J. Bryant, N. Syed, M.D. Dickey, M.J. Higgins, K. Vasilev, C.F. McConville, A.J. Christofferson, R.J. Crawford, T. Daeneke, J. Chapman, V.K. Truong, Interactions between Liquid Metal Droplets and Bacterial, Fungal, and Mammalian Cells, *Advanced Materials Interfaces* 9(7) (2022) 2102113.

- [47] J. Yang, P. Nithyanandam, S. Kanetkar, K.Y. Kwon, J. Ma, S. Im, J.-H. Oh, M. Shamsi, M. Wilkins, M. Daniele, T.-i. Kim, H.N. Nguyen, V.K. Truong, M.D. Dickey, Liquid Metal Coated Textiles with Autonomous Electrical Healing and Antibacterial Properties, *Advanced Materials Technologies* n/a(n/a) 2202183.
- [48] A. Elbourne, S. Cheeseman, P. Atkin, N.P. Truong, N. Syed, A. Zavabeti, M. Mohiuddin, D. Esrafilzadeh, D. Cozzolino, C.F. McConville, M.D. Dickey, R.J. Crawford, K. Kalantar-Zadeh, J. Chapman, T. Daeneke, V.K. Truong, Antibacterial Liquid Metals: Biofilm Treatment via Magnetic Activation, *ACS Nano* 14(1) (2020) 802-817.
- [49] B.L. He, Y.X. Du, B.W. Wang, X.Y. Zhao, S.J. Liu, Q. Ye, F. Zhou, Self-healing polydimethylsiloxane antifouling coatings based on zwitterionic polyethylenimine-functionalized gallium nanodroplets, *Chemical Engineering Journal* 427 (2022).
- [50] M. Mosina, I. Kovrljia, L. Stipniece, J. Locs, Gallium containing calcium phosphates: Potential antibacterial agents or fictitious truth, *Acta Biomaterialia* 150 (2022) 48-57.
- [51] M. Kurtjak, M. Vukomanovic, L. Kramer, D. Suvorov, Biocompatible nano-gallium/hydroxyapatite nanocomposite with antimicrobial activity, *Journal of Materials Science-Materials in Medicine* 27(11) (2016).
- [52] M. Kurtjak, M. Vukomanovic, A. Krajnc, L. Kramer, B. Turk, D. Suvorov, Designing Ga(III)-containing hydroxyapatite with antibacterial activity, *Rsc Advances* 6(114) (2016) 112839-112852.
- [53] M. Kurtjak, M. Vukomanovic, D. Suvorov, Antibacterial nanocomposite of functionalized nanogold and gallium-doped hydroxyapatite, *Materials Letters* 193 (2017) 126-129.
- [54] X.G. Chen, J.H. Zhou, Y. Qian, L.Z. Zhao, Antibacterial coatings on orthopedic implants, *Materials Today Bio* 19 (2023).
- [55] B.W. Stuart, C.A. Grant, G.E. Stan, A.C. Popa, J.J. Titman, D.M. Grant, Gallium incorporation into phosphate based glasses: Bulk and thin film properties, *J Mech Behav Biomed* 82 (2018) 371-382.
- [56] S. Yamaguchi, S. Nath, Y. Sugawara, K. Divakarla, T. Das, J. Manos, W. Chrzanowski, T. Matsushita, T. Kokubo, Two-in-One Biointerfaces-Antimicrobial and Bioactive Nanoporous Gallium Titanate Layers for Titanium Implants, *Nanomaterials-Basel* 7(8) (2017).
- [57] S. Shruti, F. Andreatta, E. Furlani, E. Marin, S. Maschio, L. Fedrizzi, Cerium, gallium and zinc containing mesoporous bioactive glass coating deposited on titanium alloy, *Appl Surf Sci* 378 (2016) 216-223.
- [58] K. Li, H.C.A. Tian, A. Guo, L.G. Jin, W.Z. Chen, B.L. Tao, Gallium (Ga)-strontium (Sr) layered double hydroxide composite coating on titanium substrates for enhanced osteogenic and antibacterial abilities, *J Biomed Mater Res A* (2021).
- [59] H. Qiao, C. Zhang, X.Y. Dang, H. Yang, Y.R. Wang, Y.L. Chen, L. Ma, S.G. Han, H. Lin, X.J. Zhang, J.P. Lan, Y. Huang, Gallium loading into a polydopamine-functionalised SrTiO₃ nanotube with Combined osteoinductive and antimicrobial activities, *Ceram Int* 45(17) (2019) 22183-22195.
- [60] J.J. Dong, D. Fang, L. Zhang, Q. Shan, Y.C. Huang, Gallium-doped titania nanotubes elicit anti-bacterial efficacy in vivo against *Escherichia coli* and *Staphylococcus aureus* biofilm, *Materialia* 5 (2019).
- [61] A. Cochis, B. Azzimonti, C. Della Valle, R. Chiesa, C.R. Arciola, L. Rimondini, Biofilm formation on titanium implants counteracted by grafting gallium and silver ions, *J Biomed Mater Res A* 103(3) (2015) 1176-1187.
- [62] B.W. Stuart, G.E. Stan, A.C. Popa, M.J. Carrington, I. Zgura, M. Necsulescu, D.M. Grant, New solutions for combatting implant bacterial infection based on silver nano-dispersed and gallium incorporated phosphate bioactive glass sputtered films: A preliminary study, *Bioact Mater* 8 (2022) 325-340.
- [63] A. Rodriguez-Contreras, D. Torres, J. Guillem-Marti, P. Sereno, M.P. Ginebra, J.A. Calero, J.M. Manero, E. Ruperez, Development of novel dual-action coatings with osteoinductive and antibacterial properties for 3D-printed titanium implants, *Surf Coat Tech* 403 (2020).
- [64] M.W. Chen, Y. Hu, Y.H. Hou, M.H. Li, L. Tan, M.H. Chen, W.B. Geng, B.L. Tao, H. Jiang, Z. Luo, K.Y. Cai, Magnesium/gallium-layered nanosheets on titanium implants mediate osteogenic differentiation of MSCs and osseointegration under osteoporotic condition, *Chem Eng J* 427 (2022).
- [65] L.A. Alberta, J. Vishnu, Y. Douest, K. Perrin, A.M. Trunfio-Sfarghiu, N. Courtois, A. Gebert, B. Ter-Ovanesian, M. Calin, Tribocorrosion behavior of β -type Ti-Nb-Ga alloys in a physiological solution, *Tribology International* 181 (2023).

- [66] L.A. Alberta, J. Vishnu, A. Hariharan, S. Pilz, A. Gebert, M. Calin, Novel low modulus beta-type Ti-Nb alloys by gallium and copper minor additions for antibacterial implant applications, *J Mater Res Technol* 20 (2022) 3306-3322.
- [67] M. Calin, A. Helth, J.J. Gutierrez Moreno, M. Bonisch, V. Brackmann, L. Giebeler, T. Gemming, C.E. Lekka, A. Gebert, R. Schnettler, J. Eckert, Elastic softening of beta-type Ti-Nb alloys by indium (In) additions, *J Mech Behav Biomed Mater* 39 (2014) 162-74.
- [68] J.-s. Wang, W.-l. Xiao, L. Ren, Y. Fu, C.-l. Ma, Effect of oxygen addition and annealing time on microstructure and mechanical properties of Ti-34Nb alloy, *Journal of Iron and Steel Research International* 30(1) (2022) 158-164.
- [69] S. Hanada, T. Ozaki, E. Takahashi, S. Watanabe, K. Yoshimi, T. Abumiya, Composition dependence of Young's modulus in beta titanium binary alloys, *Mater Sci Forum* (2003) 3103-3108.
- [70] S. Rocha, G. Adabo, G. Henriques, M. Nobilo, Vickers hardness of cast commercially pure titanium and Ti-6Al-4V alloy submitted to heat treatments, *Brazilian dental journal* 17 (2006) 126-9.
- [71] I. Cvijović-Alagić, Z. Cvijović, J. Maletaškić, M. Rakin, Initial microstructure effect on the mechanical properties of Ti-6Al-4V ELI alloy processed by high-pressure torsion, *Materials Science and Engineering: A* 736 (2018) 175-192.
- [72] Y. Wen, L. Xie, Z. Wang, L. Wang, W. Lu, L.-C. Zhang, Nanoindentation characterization on local plastic response of Ti-6Al-4V under high-load spherical indentation, *Journal of Materials Research and Technology* 8(4) (2019) 3434-3442.
- [73] X. Wang, X. Gong, K. Chou, Scanning Speed Effect on Mechanical Properties of Ti-6Al-4V Alloy Processed by Electron Beam Additive Manufacturing, *Procedia Manufacturing* 1 (2015) 287-295.
- [74] V.M. Kaoushik, U. Nichul, V. Chavan, V. Hiwarkar, Development of microstructure and high hardness of Ti6Al4V alloy fabricated using laser beam powder bed fusion: A novel sub-transus heat treatment approach, *Journal of Alloys and Compounds* 937 (2023) 168387.
- [75] L. Slokar Benić, T. Matković, P. Matković, Alloy Design and Property Evaluation of new Ti-Cr-Nb Alloys, *Materials and Design* 33 (2012) 26-30.
- [76] D. Kalita, Ł. Rogal, T. Czeppe, A. Wójcik, A. Kolano-Burian, P. Zackiewicz, B. Kania, J. Dutkiewicz, Microstructure and Mechanical Properties of Ti-Nb Alloys Prepared by Mechanical Alloying and Spark Plasma Sintering, *Journal of Materials Engineering and Performance* 29(3) (2020) 1445-1452.
- [77] A. Korneva, B. Straumal, A. Kilmametov, L. Lityńska-Dobrzyńska, R. Chulist, Ł. Gondek, P. Zięba, The Phase Transformations Induced by High-Pressure Torsion in Ti-Nb-Based Alloys, *Microscopy and Microanalysis* 28(3) (2022) 946-952.
- [78] B. Sefer, Oxidation and Alpha-Case Phenomena in Titanium Alloys used in Aerospace Industry: Ti-6Al-2Sn-4Zr-2Mo and Ti-6Al-4V, 2014.
- [79] B. Sefer, J. Roa, A. Mateo, R. Pederson, M.-L. Antti, Evaluation of the Bulk and Alpha-Case Layer Properties in Ti-6Al-4V at Micro-And Nano-Metric Length Scale, 2016, pp. 1619-1624.
- [80] H.E. Lee, J.H. Wu, C.Y. Chao, Y.H. Chang, J.K. Du, K.K. Chen, H.M. Chen, A Study of Low Young's Modulus Ti-15Ta-15Nb Alloy Using TEM Analysis, *Materials (Basel)* 13(24) (2020).
- [81] R. Raju, M. Duraiselvam, V. Petley, S. Verma, R. Rajendran, Microstructural and mechanical characterization of Ti6Al4V refurbished parts obtained by laser metal deposition, *Materials Science and Engineering: A* 643 (2015) 64-71.
- [82] A. Akman, L.A. Alberta, P.M. Giraldo-Osorno, A.B. Turner, M. Hantusch, A. Palmquist, M. Trobos, M. Calin, A. Gebert, Effect of minor gallium addition on corrosion, passivity, and antibacterial behaviour of novel β -type Ti-Nb alloys, *Journal of Materials Research and Technology* 25 (2023) 4110-4124.
- [83] E. Yılmaz, A. Gökçe, F. Findik, H.Ö. Gülsoy, Powder Metallurgy Processing of Ti-Nb Based Biomedical Alloys, *Acta Physica Polonica Series a* 134 (2018) 278-280.
- [84] B.L. Pereira, C.M. Lepienski, V. Seba, G. Hobold, P. Soares, B.S. Chee, P.A.B. Kuroda, E.S. Szameitat, L.L.d. Santos, C.R. Grandini, M. Nugent, Titanium-Niobium (Ti-xNb) Alloys with High Nb Amounts for Applications in Biomaterials, *Materials Research* 23 (2020).
- [85] A. Cremasco, P.N. Andrade, R.J. Contieri, E.S.N. Lopes, C.R.M. Afonso, R. Caram, Correlations between aging heat treatment, ω phase precipitation and mechanical properties of a cast Ti-Nb alloy, *Materials & Design* 32(4) (2011) 2387-2390.

- [86] V. Fallah, M. Amoozrezaei, N. Provas, S. Corbin, A. Khajepour, Phase-field simulation of solidification morphology in laser powder deposition of Ti–Nb alloys, *Acta Materialia* 60 (2012) 1633–1646.
- [87] L.M. Elias, S.G. Schneider, S. Schneider, H.M. Silva, F. Malvisi, Microstructural and mechanical characterization of biomedical Ti–Nb–Zr(–Ta) alloys, *Materials Science and Engineering: A* 432(1) (2006) 108–112.
- [88] R. Ummethala, P.S. Karamched, S. Rathinavelu, N. Singh, A. Aggarwal, K. Sun, E. Ivanov, L. Kollo, I. Okulov, J. Eckert, K.G. Prashanth, Selective laser melting of high-strength, low-modulus Ti–35Nb–7Zr–5Ta alloy, *Materialia* 14 (2020) 100941.
- [89] A. Muller, C. Fessele, F. Zuber, M. Rottmar, K. Maniura-Weber, Q. Ren, A.G. Guex, Gallium Complex-Functionalized P4HB Fibers: A Trojan Horse to Fight Bacterial Infection, *Acs Applied Bio Materials* 4(1) (2021) 682–691.
- [90] C.H. Goss, Y. Kaneko, L. Khuu, G.D. Anderson, S. Ravishankar, M.L. Aitken, N. Lechtzin, G. Zhou, D.M. Czyz, K. McLean, O. Olakanmi, H.A. Shuman, M. Teresi, E. Wilhelm, E. Caldwell, S.J. Salipante, D.B. Hornick, R.J. Siehnel, L. Becker, B.E. Britigan, P.K. Singh, Gallium disrupts bacterial iron metabolism and has therapeutic effects in mice and humans with lung infections, *Science Translational Medicine* 10(460) (2018) eaat7520.
- [91] F. Kurtuldu, N. Mutlu, A.R. Boccaccini, D. Galusek, Gallium containing bioactive materials: A review of anticancer, antibacterial, and osteogenic properties, *Bioactive Materials* 17 (2022) 125–146.
- [92] C. Coelho, L. Grenho, P. Gomes, P. Quadros, M. Fernandes, Nano-hydroxyapatite in oral care cosmetics: characterization and cytotoxicity assessment, *Scientific Reports* 9 (2019).
- [93] Y. Lin, Y. Liu, J. Genzer, M.D. Dickey, Shape-transformable liquid metal nanoparticles in aqueous solution, *Chemical Science* 8(5) (2017) 3832–3837.
- [94] Y. Lu, Q. Hu, Y. Lin, D.B. Pacardo, C. Wang, W. Sun, F.S. Ligler, M.D. Dickey, Z. Gu, Transformable liquid-metal nanomedicine, *Nat Commun* 6 (2015) 10066.
- [95] J. Yan, Y. Lu, G. Chen, M. Yang, Z. Gu, Advances in liquid metals for biomedical applications, *Chemical Society Reviews* 47(8) (2018) 2518–2533.
- [96] S. Houshyar, A. Rifai, R. Zizhou, C. Dekiwadia, M.A. Booth, S. John, K. Fox, V.K. Truong, Liquid metal polymer composite: Flexible, conductive, biocompatible, and antimicrobial scaffold, *J Biomed Mater Res B Appl Biomater* 110(5) (2022) 1131–1139.

APPENDICES

Appendix A

Table A. 1: Gallium coatings applied to titanium substrate and their results, as reported in literature.

Substrate	Coating(s)	Properties Investigated/ Methods	Notable Results	Ref.
Commercially pure Ti	P ₂ O ₅ -CaO-MgO-Na ₂ O-XGa ₂ O ₃ (X=6, 8.6 mol%).	Elemental mapping and microstructural analysis. Surface roughness and surface features. Mechanical properties (reduced moduli, elastic modulus, hardness). Cytocompatibility tests. Antibacterial assays.	All samples cytocompatible. Antibacterial activity effective at 24 hr for Gram-positive and Gram-negative bacteria.	[55, 62]
Ti	GaCl ₃	Surface morphology. Ion release. Antibacterial activity.	Notable antibacterial activity against A.	[56]

			<i>baumannii</i> . Up to 94.2% biofilm removal.	
Porous Ti	Ga(NO ₃) ₃	Surface characterisation. Ion release assay. Antibacterial assay. Cytotoxicity and biocompatibility assays.	Effectively inhibited <i>P. aeruginosa</i> . Effective osteogenic differentiation and mineralisation on Saos-2 cells.	[63]
Ti-6Al-4V	Mesoporous bioactive glass substituted with Ce, Ga, Zn.	Surface characterisation. Cytotoxicity and biocompatibility assays.	Homogenous and crack free coatings. Positive cytocompatibilities.	[57]
TiO ₂ nanotubes	Ga(NO ₃) ₃ -PDLA	Biofilm characterisation, cytotoxicity, and biocompatibility assays. Antibacterial assay.	Inhibition of <i>E. coli</i> and <i>S. aureus</i> bacteria.	[60]
Pure Ti sheets				
Ti	LDH-Ga and Sr	Biofilm characterisation, cytotoxicity, and biocompatibility assays. Antibacterial assay.	Enhanced differentiation of cells and osteoblasts. Antimicrobial inhibition against <i>E. coli</i> and <i>S. aureus</i> .	[58]
SrTiO ₃ nanotubes on Ti	Ga(NO ₃) ₃ -PDA	Surface characterisation. Antibacterial assay. Cytotoxicity and biocompatibility assays.	Superior osteoinductive activity. Gradual and constant antibacterial agent release of <i>E. coli</i> and <i>S. aureus</i> . Almost no bacteria after 7 days.	[59]
Ti	Ga(NO ₃) ₃	Surface characterisation. Cytotoxicity, osteogenesis and osteoclastic biocompatibility assays.	Promoted osteogenesis, suppressed osteoclast generation.	[64]
Grade 2 Ti	GaCis and GaOss (Ga(NO ₃) ₃)	Morphological characterisation. Mechanical properties (elastic modulus, hardness). Antibacterial assay. Cytotoxicity and biocompatibility assays.	Strong inhibition of 27-35% against metabolic activity. Inhibition of <i>A. baumannii</i> . Good cytocompatibilities.	[14, 61]

Table A. 2: Addition of gallium metallurgically added to titanium, including key methods and results.

Chemical Composition (wt%)	Properties Investigated/ Methods	Notable Results	Ref.
Ti-8Al-3Si-3Zr-1Ga Ti-8Al-3Si-3Zr-2Ga Ti-8Al-3Si-3Zr-20Ga	Microstructural analysis. Antibacterial assays. Biocompatibility/ cytotoxicity assays.	Inhibition of <i>S. aureus</i> , more than 80% reduction in the metabolic activity. Potent antibacterial efficiency for all samples, even 1-2 wt% additions of Ga. Great cytocompatibilities.	[15]
Ti-45Nb-2Ga Ti-45Nb-4Ga Ti-45Nb-6Ga Ti-45Nb-8Ga	Chemical composition analysis. Mechanical properties (yield strength, Young's modulus, hardness, ductility).	4 wt% Ga depicted the best combination of mechanical properties. 40% increase in strength over Ti-45Nb. Maximum yield strength: 620 ± 2 MPa. Microhardness: 232 ± 5 HV. Young's modulus: $73 \div 82$ GPa. Maximum ductility: 32%	[9, 66]
Ti-45Nb-4Ga Ti-45Nb-8Ga	Microstructural analysis. Mechanical properties. Corrosion and Tribocorrosion properties.	Single β phase. Ga caused no deleterious effect on the corrosion resistance.	[66]

Appendix B

Table B. 1: Literature review of Ti-Nb alloys found in the literature and their reported mechanical properties.

Reference	Alloy(s) (%wt)	E (GPa)	Yield Strength (MPa)	UTS (MPa)
https://www	(Ti-45Nb)96-4Ga	77.7 ± 3.3	681	675 ± 8
	(Ti-45Nb)96-4Cu	73.4 ± 1.9	539	544 ± 10
	(Ti-45Nb)96-2Ga-2Cu	78.5 ± 2.5	596	612 ± 11
https://www	98(Ti-45Nb)-2Ga	73.0 ± 2.8	551 ± 3	
	96(Ti-45Nb)-4Ga	77.0 ± 3.1	681 ± 8	
	94(Ti-45Nb)-6Ga	78.1 ± 3.1	602 ± 10	
	92(Ti-45Nb)-8Ga	82.5 ± 2.2	620 ± 2	
https://www	Ti-34Nb-25Zr	62 ± 3.6	810 ± 48.0	839 ± 31.8
	Ti-30Nb-32Zr	65 ± 4.2	782 ± 18.8	794 ± 10.1
	Ti-28Nb-35.4Zr	64 ± 4.5	729 ± 26.3	755 ± 28.3
	Ti-24.8Nb-40.7Zr	63 ± 4.2	682 ± 52.9	704 ± 49.5
https://iopscience	Ti-35Nb-5Zr	59.8	~510	~650
	Ti-35Nb-10Zr	58.8	~490	~600
	Ti-35Nb-15Zr	62.9	689.13	718
https://www	Ti-24Nb-4Zr-7.9Sn	42		850
https://iopscience	Ti-35Nb-3Zr-2Ta	48		880
https://www	(Ti-40Nb)-3.5In	51	568	1074
	(Ti-40Nb)-5In	49	511	775
https://www	Ti-32Nb-2Sn	68	640 ± 20	760 ± 30
	Ti-32Nb-4Sn	64	460 ± 20	640 ± 15
https://www	96(Ti-45Nb)-4Ga	69.4		
	92(Ti-45Nb)-8Ga	79.1		
https://www	Ti-24Nb-4Zr-7.5Sn	52		
https://onlin	Ti-35Nb-7Zr-5Ta	55	814	834
https://www	Ti-25Nb-25Ta	55		530
https://www	Ti-24 at% Nb-2 at% Zr	64		710
	Ti-24 at% Nb-4 at% Zr	62		600
https://www	Ti24Nb2Zr (at%)	62	345	440
	Ti20Nb6Zr	60	365	470
	Ti18Nb8Zr	75	455	550
	Ti16Nb10Zr	70	485	520
https://www	Ti-12Mo-6Zr-2Fe	74-85	1000-1060	1060-1100
	Ti-15Mo-5Zr-3Al	75	870-968	882-975
	Ti-35Nb-5Ta-7Zr	55	547	597
	Ti-35Nb-5Ta-7Zr-0.4O	66	976	1010
	(Ti-35Nb)-4Sn	42-55	619-787	673-846
	Ti-13Nb-13Zr (aged)	79-84	836-908	973-1037
	Ti-24-Nb-4Zr-7.9Sn	42	≈350	850
	Ti-29Nb-13Ta-4.6Zr	55-65	864	911
Ti-28Nb-13Zr-0.5Fe	58-120	780-1050		
Ti-25Nb-3Zr-3Mo-2Sn	50-80	440-500	708-715	
https://www	Ti-41.1Nb-7.1Zr	65 ± 1	490 ± 27	490 ± 27
	Ti-35.3Nb-7.1Zr-5.1Ta	63 ± 2	550 ± 10	550 ± 10
https://www	Ti-35Nb-2Ta-3Zr	47.63	460.59 to 576.91	
https://www	Ti-22.5Nb-0.7Ta-2Zr-1.0O (at.%)	65		750
https://link	Ti-25Nb-2Ta-3Zr	75.2		864
	Ti-30Nb-2Ta-3Zr	57.1		663
	Ti-35Nb-2Ta-3Zr	52		431
	Ti-40Nb-2Ta-3Zr	57.8		589
https://link	Ti-29Nb-13Ta-4.6Zr @ 723K	71	742	788
	Ti-29Nb-13Ta-4.6Zr @ 823K	58	355	663
https://www	Ti-35Nb-7Zr-5Ta	81		630
https://www	Ti-35.3Nb-7.1Zr-5.1Ta	63 ± 2	550 ± 10	550 ± 10
	Ti-41.1Nb-7.1Zr	65 ± 1	490 ± 27	490 ± 27
https://www	Ti-24Nb-3Ga %mol			510-550
https://www	Ti-38Nb-0.2O	50 ± 3	316 ± 9	620 ± 21
	Ti-38Nb-0.5O	52 ± 2	1141 ± 17	1218 ± 48

Appendix C

Table C. 1: The three-step automatic grinding and polishing method for the developed alloys, together with reference Ti-6Al-4V [97].

	Grinding		Polishing
Surface	MD-Mezzo	MD-Largo	MD-Chem
Abrasive	Type: Diamond Size: #220	Type: Diamond Size: 9 μm	Type: Colloidal Silica Size: 0.25 μm
Suspension/ Lubricant	Water	DiaPro Allegro/Largo 9	90% OP-S & 10-30% H2O2
rpm	300	150	150
Force (N)	25	30	30
Time (min)	Until Plane	5	7

Appendix D

Table D. 1: Raw results for the microhardness tests.

Indent	Microhardness (HV)		
	Ti-33Nb-3Ga	Ti-33Nb-5Ga	Ti-6Al-4V
1	218	270	297
2	217	264	296
3	217	251	297
4	218	267	301
5	221	251	295
6	222	271	296
7	213	252	297
Mean	218.00	260.86	297.00
STDEV	2.94	9.19	1.91

Table D. 2: Raw nanoindentation results.

Indent	Ti-33Nb-3Ga		Ti-33Nb-5Ga		Ti-6Al-4V	
	HV (Vickers)	E (GPa)	HV (Vickers)	E (GPa)	HV (Vickers)	E (GPa)
1	<i>Omitted</i>		251.993	70.9463	365.993	118.1099
2			266.193	68.4819	370.039	117.9356
3			266.254	67.8608	397.206	121.9576
4	225.302	80.1089	271.73	66.5774	371.586	122.3153
5	228.904	77.4817	270.994	66.825	350.153	117.872
6	237.291	74.9575	275.916	67.8633	390.547	122.9867
7	229.635	75.5944	274.287	65.6901	374.469	121.7821
8	220.038	73.1601	<i>Omitted</i>		363.44	120.1281
9	244.968	75.4865	264.902	64.8268	367.624	118.4065
10	259.812	77.278	287.359	65.5257	376.706	121.4689
11	235.663	72.2626	283.066	67.8521	373.961	121.0695
12	246.172	75.5829	279.468	66.1505	386.793	118.2955
13	249.19	74.6153	284.198	68.5038	364.264	125.8822
14	256.004	75.8822	286.921	67.6088	350.394	119.8245
15	256.871	76.4234	277.348	65.858	<i>Omitted</i>	
16	223.997	70.7734	<i>Omitted</i>		367.588	118.7649
Mean	239.53	75.35	274.33	67.18	371.38	120.45
STDEV	13.56	2.39	9.91	1.59	13.04	2.32

Table D. 3: Raw results for the antimicrobial activity assay.

	<i>P. aeruginosa</i> (3h)			Mean	STDEV
Ti	1	5	3	3	2
3%	90	95	85	90	5
5%	95	98	92	95	3
	<i>S. aureus</i> (3h)			Mean	STDEV
Ti	3	1	2	2	1
3%	30	35	45	36.67	7.64
5%	45	50	55	50	5
	<i>P. aeruginosa</i> (24h)			Mean	STDEV
Ti	5	6	8	6.33	1.53
3%	30	25	35	30	5
5%	95	90	92	92.33	2.52
	<i>S. aureus</i> (24h)			Mean	STDEV
Ti	3	5	6	4.67	1.53
3%	30	40	20	30	10
5%	50	60	40	50	10

Appendix E

Flinders UNIVERSITY RISK ASSESSMENT FORM

List identified hazards and detail measures taken to eliminate / minimise the risks:
(boxes on this form will expand to fit text)

Click to add image

Risk Assessment No.	
Reference to SWP/SWMS No.	

College/Portfolio	Science and Engineering	Area/Unit	CSEM	Location	3.19 Tonsley	Area/Unit Manager	
Task/Procedure	Struers Tegramin-25 Polisher	Workers consulted / involved		Date	29/03/2023	Review Date	

Identified Hazard before controls		Risk Assessment			Risk Controls	Residual risk			Implementation
No.	Description	Consequences	Likelihood	Risk Measure (see matrix)	Control measures	Consequences	Likelihood	Risk Measure (see matrix)	Date controls implemented / reviewed
1	Electrical Exposure	Major Injury	Highly Unlik	Medium	Ensure that electrical equipment is tested and tagged. Visually inspect cables to detect any damage prior to use.	Major Injury	Highly Unlik	Medium	29/03/2023
2	Ejected Workpiece	Minor Injury	Highly Unlik	Medium	Ensure the interlock cover is closed prior to any polishing step. Wear safety glasses.	First Aid	Highly Unlik	Low	29/03/2023
3	Skin coming into contact with polishing solutions	Negligible	Possible	Low	Wear gloves and lab coat or long sleeved top. If solution contacts skin, wash with large amount of water.	Negligible	Possible	Low	29/03/2023
4		-Select -	- Select -			- Select -	- Select -		

Review the risk measured, and the controls implemented are still relevant and effective, then please select one of the following:

- A The assessment reveals that the potential risk to health and safety from the use of the plant/equipment/procedure is not currently significant.
- B The assessment reveals that the potential risk to health and safety from the use of the plant/equipment/procedure is significant. However controls are in place that reduce risk as low as is reasonably practicable.

Note: If the risk level is still Extreme/High after controls are in place, then cease the activity, identify and implement further controls and consult with your manager/supervisor until the risk is reduced as low as reasonably practicable.

Figure E. 1: Risk assessment form for the polishing machine.

Flinders UNIVERSITY RISK ASSESSMENT FORM

List identified hazards and detail measures taken to eliminate / minimise the risks:
(boxes on this form will expand to fit text)

Click to add image

Risk Assessment No.	
Reference to SWP/SWMS No.	

College/Portfolio	Science and Engineering	Area/Unit	CSEM	Location	Bedford Park	Area/Unit Manager	
Task/Procedure	Scanning Electron Microscope + EDS	Workers consulted / involved		Date	29/03/2023	Review Date	

Identified Hazard before controls		Risk Assessment			Risk Controls	Residual risk			Implementation
No.	Description	Consequences	Likelihood	Risk Measure (see matrix)	Control measures	Consequences	Likelihood	Risk Measure (see matrix)	Date controls implemented / reviewed
1	Electrical Exposure	Major Injury	Highly Unlik	Medium	Ensure that electrical equipment is tested and tagged. Visually inspect cables to detect any damage prior to use.	Major Injury	Highly Unlik	Medium	29/03/2023
2	Ionising Radiation Exposure	Minor Injury	Highly Unlik	Medium	Ensure annual servicing is implemented and machine is checked for EM radiation. Ensure interlock enclosures are closed. Ensure warning devices are fitted and tested and tagged.	Negligible	Highly Unlik	Low	29/03/2023
3	Vacuum Oil	Major Injury	Highly Unlik	Medium	Dispose of oil safely as per chemical waste procedures. Wear safety glasses, gloves and a lab coat.	Minor Injury	Highly Unlik	Medium	29/03/2023
4		-Select -	- Select -			- Select -	- Select -		

Review the risk measured, and the controls implemented are still relevant and effective, then please select one of the following:

- A The assessment reveals that the potential risk to health and safety from the use of the plant/equipment/procedure is not currently significant.
- B The assessment reveals that the potential risk to health and safety from the use of the plant/equipment/procedure is significant. However controls are in place that reduce risk as low as is reasonably practicable.

Note: If the risk level is still Extreme/High after controls are in place, then cease the activity, identify and implement further controls and consult with your manager/supervisor until the risk is reduced as low as reasonably practicable.

Figure E. 2: Risk assessment form for the SEM and EDS.